AIAA JOURNAL
Vol. 52, No. 5, May 2014

Nonlinear Analysis of PrandtlPlane Joined Wings: Effects of Anisotropy

Rauno Cavallaro,* Luciano Demasi,† and Andrea Passariello‡
San Diego State University, San Diego, California 92182

DOI: 10.2514/1.J052242

Structural geometrical nonlinearities strongly affect the response of joined wings: it has been shown that buckling evaluations using linear methods are unreliable, and only a fully nonlinear stability analysis can safely identify the unstable state. This work focuses on the understanding of the main physical mechanisms driving the wing system's response and the snap-buckling instability. Several counterintuitive effects typical of unconventional nonplanar wing systems are discussed and explained. In particular, an appropriate design of the joint-to-wing connection may reduce the amount of bending moment transferred, and this is shown to eventually improve the stability properties, although at price of a reduced stiffness. It is also demonstrated that the lower-to-upper-wing stiffness ratio and the torsional–bending coupling, due to both the geometrical layout and anisotropy of the composite laminates, present a major impact on the nonlinear response. The findings of this work could provide useful indications to develop effective aeroelastic reduced-order models tailored for airplane configurations experiencing important geometric nonlinearities such as PrandtlPlane, truss-braced and strut-braced wings, and sensorcraft.

I. Introduction

JOINED wings were proposed in the 1970s [1–3] for commercial transport and supersonic fighters. Joined wings were also the subject of U.S. [4,5] and European [6] patents. Many advantages are claimed when compared to classical cantilevered configurations [7,8]: improved stiffness properties, high aerodynamic efficiency [9], and superior stability and control characteristics. In addition to these theoretically significant advantages, a diamond joined wing can enclose a large antenna and be used for high-altitude surveillance [10].

For civil transportation, the PrandtlPlane has been analyzed in terms of aerodynamic performances, flight mechanics and controls, dynamic aeroelastic stability properties, and preliminary design [5,11].

The design of a joined-wing type of aircraft for civil transportation was also adopted in the U.S. with the introduction of the concepts of strut-braced wings [12] and truss-braced wings [13].

The growth of interest in joined wings led to both experimental [14,15] and theoretical [16,17] studies. These studies showed that the tools developed in decades, and effectively used by the industry to analyze classical cantilevered wings, need to take into account structural nonlinearities [18,19], which are significant even for small angles of attack and attached flow. The significant forces and moments transferred through the joint make the geometric structural effects particularly important, and linear aeroelastic models [20] can give only qualitative information on the instability properties, but they may miss important structural effects, which should be taken into account [21,22]. However, the adoption of fully nonlinear, structural models is impractical for design purposes, especially if several alternative configurations are explored in an optimization [20] effort. Ideally, the designer should have access to efficient reduced-order models. However, even well-established reduced-order techniques [23] based on second-order modes [24,25] performed in an unsatisfactory manner when applied to joined-wing cases [23,26].

It was then realized that, in order to effectively build a reduced-order aeroelastic model specifically tailored for an efficient simulation with a full inclusion of the structural geometric effects, a physical understanding of the mechanism driving the nonlinear response of joined wings should be achieved. This is pursued in this work.

II. Contributions of the Present Work

PrandtlPlane configurations are joined-wing aircraft designed for civil transportation. Thus, global snap-buckling instabilities are not acceptable. However, as discussed in [27] and in this work, a snap buckling can take place even after a quasi-linear load-displacement response. This demonstrates the necessity of an understanding of the physics behind the instability phenomenon to avoid an abrupt change of state after a response that appeared to be linear.

For the PrandtlPlane-like configuration, an investigation was pursued in [27]. The main results that were found could be summarized in the following main aspects:

1) The strong nonlinear structural effects make the linear buckling analysis not very reliable as far as the static critical condition is concerned.

2) The system may be sensitive to a snap-buckling type of instability under a certain combination of structural parameters. This led to the definition of the so-called snap-buckling region, which gives important indications on the design of these configurations.

3) It was shown that the load repartition between the upper and lower wings has a significant impact on the stability conditions: for a typical sweptback lower-wing and sweptforward upper-wing configuration, more load on the upper wing (UW) alleviates the risk of instability.

4) Some counterintuitive effects typical of this layout were discovered. For example, increasing the joint's size may be considered a not-efficient design since it could increase the height, and this would appear unfavorable: it is well known that slender columns may increase the tendency to buckle. However, for aerodynamiclike mechanical loadings, it was shown that the complex nonlinear response of the joined wing actually has an opposite effect and the stability properties are improved when the joint's height is increased. This also has practical implications since the induced drag

Presented as Paper 2012-1462 at the 53rd AIAA SDM Conference, Honolulu, HI, 23–26 April 2012; received 14 September 2012; revision received 31 July 2013; accepted for publication 17 October 2013; published online 27 March 2014.

*Ph.D. Candidate, Department of Aerospace Engineering, San Diego State University and Department of Structural Engineering, University of California, San Diego.

†Associate Professor, Department of Aerospace Engineering. Member AIAA.

‡Visiting Graduate Student; also M.S. Candidate, Dipartimento di Ingegneria Aerospaziale, Università di Pisa, 56126 Pisa, Italy.

is significantly reduced when the gap between the upper and lower wings is increased.

5) Increasing the sweep angles was shown to dramatically reduce the snap-instability load.

These findings had relevant practical implications, but several questions needed an answer. In particular, the effects of composite materials required investigation since additional couplings could be introduced because of the anisotropy. Moreover, currently, the adoption of composites is increasingly relevant (the new Boeing 787 and the Airbus 350 present a large percentage of structures designed with composites) and has to be considered for joined wings (JWs). In addition, even for isotropic materials but general geometries (sweep angles, dihedrals, built-in twist), a realistic PrandtlPlane would present strong anisotropic behavior from a global point of view.

In the design of these configurations, an equivalent composite plate model [28] could provide important indications. Thus, the present investigations based on platelike models for the wings and the joint could also provide practical design information.

The JW models discussed and investigated in this work do not intend to reproduce the complex stiffness distributions of a realistic airplane configuration. The material properties and geometric dimensions are selected to be consistent with the ones typically adopted in wind-tunnel models. Moreover, the materials are modified to explore how the different stiffness distributions affect the nonlinear response, with particular emphasis on the snap-buckling instability.

This paper will provide contributions toward a fundamental understanding of the nonlinear response of PrandtlPlane joined wings. The first contribution concerns the role of the anisotropy (introduced by adopting composite materials) on the nonlinear response, with particular emphasis on the snap-buckling instability. The second contribution is about the effects of the joint-wing connection (boundary conditions) on the geometrically nonlinear structural behavior. As suggested in [29], since the system is statically indeterminate, significant reaction loads can build up in the joint area that could have important consequences on stiffness and stability. Changing the wing-to-wing connection helps to isolate and better understand the phenomenon. The third contribution is finding the main driving mechanism that leads to the instability. It is shown that the bending moment transferring through the joint is determinant. Interesting features typical of the configurations that experience buckling are discussed, with particular emphasis on the inward bending of the upper wing and rigid rotation of the joint in both chordwise and spanwise directions. The fourth contribution is about the importance of the differential stiffness of the two wings: it will be shown that the stiffness ratio is one of the major parameters determining the instability risks. The upper wing (usually compressed under typical load conditions) needs to have a smaller relative stiffness: a surprising result with important implications.

The present work provides indications on the physical mechanisms of the nonlinear instability for PrandtlPlane configurations and joined wings. This could have practical application in the development of new and efficient aeroelastic reduced-order models, which could effectively adopt existing and reliable tools already in use in the aerospace industry but cannot be directly extended for the joined wings without a proper understanding of the nonlinear phenomena.

III. Nonlinear Structural Model

The geometrically nonlinear finite element [30] is based on the linear membrane constant strain triangle and the flat triangular plate element. Structural tangent matrix $\boldsymbol{K}_T$ is the sum of two contributions: the elastic stiffness matrix $\boldsymbol{K}_E$ and the geometrical stiffness matrix $\boldsymbol{K}_G$.

The nonlinear governing equations are solved by adopting iterative methods such as Newton–Raphson and arclength techniques [31]. After each iteration, a displacement vector is obtained, rigid-body motion is eliminated from the elements, and the pure elastic rotations and strains are found [30]. Using these quantities, the internal forces are updated for the next iteration.

The key relation that needs to be solved at each iteration [27,32] involves the structural tangent matrix $\boldsymbol{K}_T^{\text{step}\mu\text{iter}n}$. $\boldsymbol{u}^{\text{step}\mu\text{iter}n}$, the external nonfollower loads $\boldsymbol{P}_{\text{ext}}$, and the array $\boldsymbol{P}_{\text{unb}}^{\text{step}\mu\text{iter}n}$ containing the unbalanced loads

$$\boldsymbol{K}_T^{\text{step}\mu\text{iter}n} \cdot \boldsymbol{u}^{\text{step}\mu\text{iter}n} = \underbrace{(\Lambda^{\text{step}\mu\text{iter}(n+1)} - \Lambda^{\text{step}\mu\text{iter}n})}_{\lambda^{\text{step}\mu\text{iter}n}} \boldsymbol{P}_{\text{ext}} + \boldsymbol{P}_{\text{unb}}^{\text{step}\mu\text{iter}n} \tag{1}$$

where the displacement $\boldsymbol{u}^{\text{step}\mu\text{iter}n}$ and, for the arclength case, the applied load fraction $\Lambda^{\text{step}\mu\text{iter}(n+1)}$ are unknown. Different closing constraint equations could be employed, leading to different arclength methods, such as Crisfield's, Riks'Wempner, or Ramm's (also called modified Riks) methods [31]. As an example, application of Crisfield's cylindrical arclength method [31] leads to the following constraint:

$$\|\boldsymbol{u}^{\text{step}\mu\text{iter}n} + \boldsymbol{U}^{\text{step}\mu\text{iter}n} - \boldsymbol{U}^{\text{step}\mu\text{iter}1}\|^2 = \Delta l^2 \tag{2}$$

where Δl has been previously fixed. Equations (1) and (2) give rise to a second-order relation for $\lambda^{\text{step}\mu\text{iter}n}$.

It is worth noticing that the success of one of the arclength strategies in overcoming limit points is problem dependent. In some cases, some strategies perform better than others; thus, it may be necessary to switch between them to track the whole response curve.

The postcritical numerical analyses are inherently difficult to carry out. It has been the authors' experience that a satisfactory performance of the finite element (FE) formulation in the precritical region does not imply a satisfactory performance on the postcritical region. Several numerical investigations showed that the terms of the out-of-plane contribution to the geometric stiffness matrix are crucially important on this regard.

Generally, Newton–Raphson procedures are preferred for computation of states far from limit points, for robustness and efficiency reasons. Moreover, to effectively track the curve beyond limit points, it is necessary to adopt an arclength technique; and restarting the analysis from a converged state (restart capability), with the adoption of different set of parameters, may be necessary. This is the reason why an efficient technique that significantly reduces the needs of restarting analyses was implemented. In particular, the capability used in this work can automatically switch from Newton–Raphson to arclength strategies when close to a limit point. The opposite capacity to switch back to the Newton–Raphson technique when far from limit points was also implemented. Furthermore, an automatic switch to different arclength techniques when the current one fails to overcome a limit point is also possible. More details are described in [27,32].

IV. Description of Analyzed Joined-Wing Configurations

Swept wings present a significant coupling between the bending and torsional deformations with important aeroelastic consequences [33]. Due to the overconstrained nature of the joined wings, the sweep angle effects are even more determinant, since the upper and lower wings are joined at the tip and the resulting structure is overconstrained. The bending–torsion coupling is more complex than a simple cantilevered wing and directly affects the stability properties and postcritical behavior of these configurations. Moreover, the composites can introduce some couplings that are not present in the case of isotropic materials; and with an accurate design, the bending and torsional deformations may be modified to improve the overall response.

This work is mainly focused on the fundamental understanding of the geometric structural nonlinearity and the role it plays in the static instability for both unswept and swept joined wings. With this in mind, two configurations are discussed and analyzed. The first configuration is an unswept joined wing (Fig. 1), and the second one (Fig. 2) is a more realistic joined wing that presents a sweptback lower wing (LW) and a sweptforward upper wing. The loading

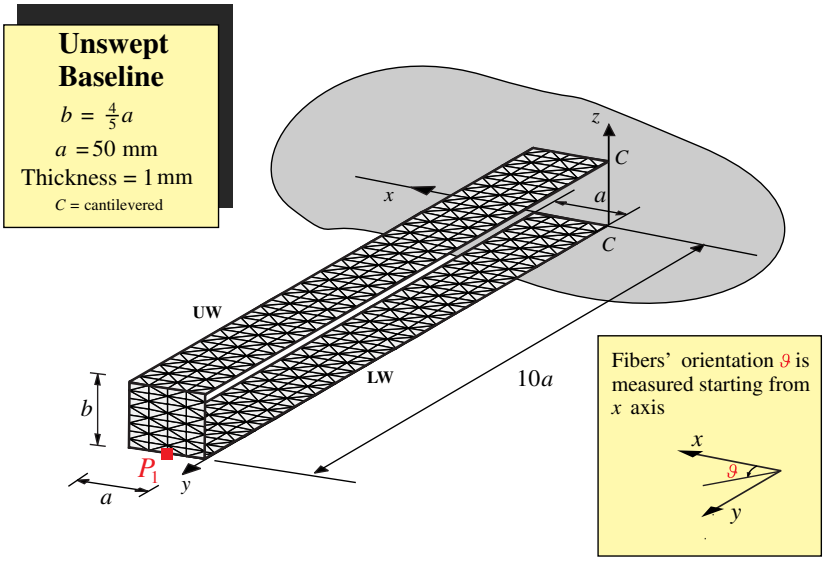

Fig. 1 Unswept baseline configuration.

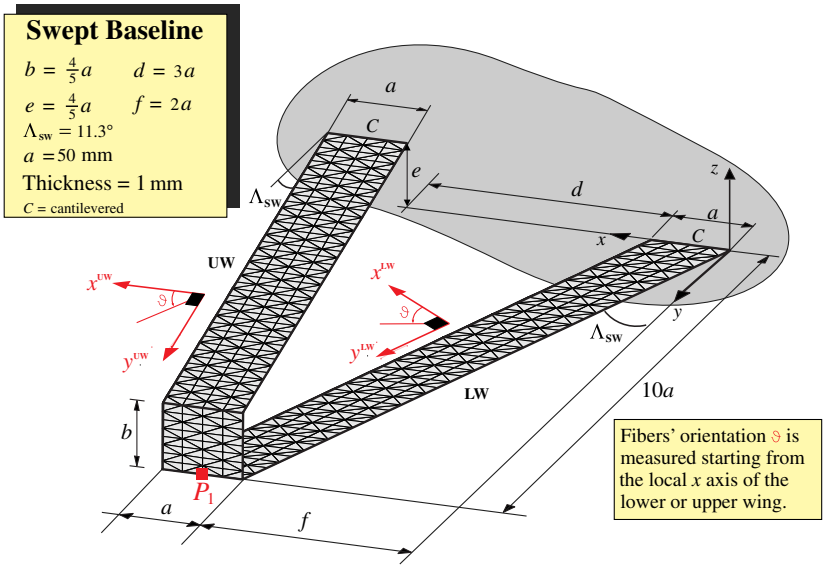

Fig. 2 Swept baseline configuration.

condition is represented by a nonaerodynamic conservative vertical pressure (direction $+z$) applied to both the upper and lower wings' surfaces (the joint is unloaded). The magnitude of the pressure is $p_z = 0.55125$ kg/mm $\cdot$ s^2 and corresponds to a dynamic pressure relative to a speed of $V_\infty = 30$ m/s. The thickness is held constant for both the wings and the joint and is equal to 1 mm. Several materials will be adopted in this work to investigate the effects of composites on the nonlinear postcritical behavior of the joined wings. For a meaningful comparison of their effects, two baseline configurations are defined for both the unswept and swept geometries reported in Figs. 1 and 2. In particular, each baseline configuration presents a Young's modulus of $E_{\text{REF}} = 6.9 \cdot 10^7$ kg/mm $\cdot$ s^2 and a Poisson's ratio of $\nu_{\text{REF}} = 0.33$. The shear modulus is calculated from the well-known relation $G_{\text{REF}} = E_{\text{REF}}/2(1 + \nu_{\text{REF}})$. The baseline configurations are referred to as UREF and SREF for the unswept and swept cases, respectively.

The results discussed in this work will present several investigations in which multilayer composite materials are adopted. For these cases, the laminates' thicknesses are kept constant, whereas the lamination schemes are changed. Each lamina or ply is identified by a material coordinate system that is, in general, not coincident with the global coordinate system adopted in the solution of the problem. For that reason, it is necessary to specify the fibers' orientation angle at ply level. In this work, the angle is measured starting from the wing's local x axis: in the unswept case, it coincides with the global x axis (see Fig. 1), whereas for the swept case, each wing has its own local reference x axis (x^{UW} and x^{LW} for the upper and lower wings, respectively: see Fig. 2). The local x axis is always perpendicular to the wingspan direction and is not parallel to x in the general case of a swept joined wing.

A snapping phenomenon at global structural level (see also [27]), as the ones that will be discussed here, could not be accepted. It is also true that, when possible, the structures in aeronautical engineering are designed to have a linear response. According to these observations, it may be stated (incorrectly) that a structural analysis may lose interest well before a limit point is reached (see [34] for a discussion about risks related to bistable regions).

It may also be argued that the configurations for which snap occurs are subjected to a deformation that would not be realistic for a joined-wing aircraft.

However, the following observations could be made:

1) The choices of dimensions of the baseline models (see Figs. 1 and 2) have been selected to be consistent with wind-tunnel scaled models.

2) The loads have been accordingly selected to observe the instability phenomenon, in an effort of conceptual understanding of

the geometric nonlinearities and the effects of composite materials for both swept and unswept configurations.

3) High-altitude long-endurance configurations typically undergo very large deformations; see, for example, [35].

4) The knowledge of different static equilibrium configurations at the same load level is very important for a thorough stability analysis [34].

The focus is on the understanding of the snap-buckling phenomenon [27] and how the adoption of composite materials changes the strongly nonlinear structural behavior. A snap-buckling occurrence should be avoided. Composites provide a very effective option for the designer. How this can be practically achieved is extensively assessed in this work.

It should be pointed out that the efficient design of composite platelike wings in view of achieving an optimal response (e.g., quasi-linear or snap-buckling-free response) has practical implications since a real wing–box structure could be eventually analyzed with an equivalent plate representation [28]. Thus, the analyses reported in this work could be adopted to gain directions about the design of a real snap-free joined-wing structure.

The main objective of this work is to shed some light on the physics related to the highly complex critical and postcritical behavior of a composite anisotropic joined wing. Thus, the material properties used in the investigations are artificially modified to gain insights on the actual structural parameters that affect the structural response.

V. Unswept Joined-Wing Cases

A. General Concepts

The unswept cases present the geometry shown in Fig. 1, whereas the material properties are changed case by case to identify the important parameters affecting the nonlinear response. The joint transfers forces and moments between the wings. Thus, it is intuitive to expect a significant influence of the extensional and bending stiffness on the snap-buckling and postcritical responses. In this regard, if one considers the analogy with Euler's column and its instability properties when subjected to compressive forces, it could be inferred that, when the two wings are loaded with a vertical pressure in the $+z$ direction, the consequent compression of the upper wing is the driving mechanism to the instability. Thus, a design strategy aimed at increasing the extensional stiffness could be suggested. Actually, in this work, a counterintuitive result will be demonstrated: the bending stiffness is the most relevant parameter that could not be easily predicted by simply using the joined-wing-analog argument of Euler's column instability. Moreover, it will be shown that the bending stiffness ratio between the lower and upper wings is what regulates the snap buckling for the unswept configuration reported in Fig. 1.

B. Lower-to-Upper Wing Stiffness Ratio and its Effects on Snap Buckling

The isotropic, orthotropic, and anisotropic cases are now investigated.

1. *Isotropic Case*

The Young's moduli of the upper and lower wing were varied to change the stiffness ratio but in such a way as to maintain the linear response of point P1 of the UREF configuration; for details about the analytical expression, see Appendix A of [27]. In the process of varying the material of the wings (see Table 1), the joint's material has been held the same. All the analyses with the present software have been validated with NASTRAN, and the agreement is excellent. However, in many cases, it was not possible to drive to convergence the commercial tool after the limit point: this is an indication of the numerical difficulties associated with these types of simulations for the case of joined wings and the necessity of the automatic switching features (from Newton–Raphson to arclength, and vice versa) implemented in the in-house capability. From Table 1 and the figures reported in [32] (omitted here for brevity), it can also be observed that the lower-to-upper wing stiffness ratio $E^r = E^{\mathrm{LW}}/E^{\mathrm{UW}}$ plays an important role in determining the nonlinear response and snap phenomenon occurrence: increasing E^r raises the snap load level (i.e., the first limit point encountered when tracking the response curve occurs at higher values of the load parameter Λ). Further increasing of the stiffness ratio E^r postpones the buckling occurrence to higher-level loads; eventually, it disappears and the response presents a stiffening effect (increasing of the load parameter/displacement slope). As Table 1 suggests, a critical value E^r_{CR} could be defined that, for this particular case, is equal to 2.5.

From the definition of E^r, it is deduced that increasing the stiffness of the lower wing compared to the stiffness of the upper wing is beneficial as far as the elimination of the snap buckling is concerned. This is apparently a counterintuitive result since it would be expected that increasing the stiffness of the upper wing (the one which is compressed under this load condition) could be beneficial. It also confirms the fact that, for joined wings, the type of response does not follow the interpretation that could be used by adopting the classical arguments of the Eulerian compressed column. For an assigned load level, comparison of the deformed shapes corresponding to different values for the parameter E^r showed [32] that the configurations on the verge of snapping (for that load level) present a deformation of the upper wing characterized by a more pronounced inward bending deformation. This property is derived here for the isotropic case, but its validity is more general, as the discussion regarding the orthotropic materials will show.

Summarizing, to avoid snap-buckling, the ratio E^r is one of the dominant parameters. In particular, a configuration featuring a value of this parameter larger than a critical value E^r_{CR} does not present a snap-buckling problem.

A stiffer lower wing (or alternatively, a more compliant upper wing) is then desirable for avoiding the snap-buckling problem. In a real design, the different stiffness of the two wings is likely to be connected with a difference share of the load carried by each wing. This also presents implications on the stress levels reached by the structure and has to be properly taken into account when these types of configurations are designed.

2. *Orthotropic Case*

It should be observed that an isotropic material does not present a preferential direction; thus, the nature of the nonlinear response can be fully investigated only if anisotropic materials are adopted. As a

Table 1 Cases and relative parameters: details about materials used for different configurations [a]

Case identification (ID)	Wing	Young's modulus $E \times 10^{-7}$, kg/mm · s^2	Ratio $E^r = E^{\mathrm{LW}}/E^{\mathrm{UW}}$	Snap	Critical load Λ^{CR}
UREF	Upper	6.9	1	Yes	0.91
	Lower	6.9			
UISO1	Upper	12	0.2	Yes	0.81
	Lower	2.4			
UISO2	Upper	10	0.4	Yes	0.84
	Lower	4.1			
UISO3	Upper	8.7	0.6	Yes	0.86
	Lower	5.2			
UISO4	Upper	7.7	0.8	Yes	0.88
	Lower	6.1			
UISO5	Upper	6.0	1.3	Yes	0.95
	Lower	7.8			
UISO6	Upper	5.0	1.8	Yes	1.07
	Lower	8.9			
UISO7	Upper	4.5	2.1	Yes	1.22
	Lower	9.5			
UISO8	Upper	4.1	2.4	Yes	1.52
	Lower	9.9			
UISO9	Upper	4.1	2.45	Yes	1.68
	Lower	10			
UISO10	Upper	4.0	2.5	No	∞
	Lower	10.1			

[a]Poisson's ratio is $\nu = 0.33$ for all cases.

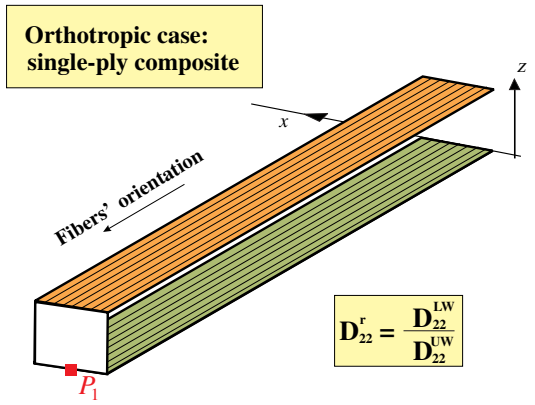

Fig. 3 Unswept configurations for orthotropic cases and definition of lower-to-upper wing stiffness ratio.

first step toward this direction, the case of orthotropic plates is here analyzed.

The first test case involves a single lamina with fibers directed along the wingspan. The fibers' angle ϑ, measured counterclockwise from the x axis, is equal to 90 deg; see Fig. 3. This choice makes the material behavior orthotropic with respect to the freestream x and spanwise y directions.

As done for the previously discussed isotropic case, the material properties are changed to numerically test the influence of the different parameters. However, modification of the properties is performed without changing point P_1 linear static response. This choice is useful for meaningful comparison of the different responses.

The material properties are selected as follows: $E_2^{LW} = E_2^{UW} = E_{REF}$, $G_{12}^{LW} = G_{12}^{UW} = G_{REF}$, and $\nu_{12}^{LW} = \nu_{12}^{UW} = \nu_{REF}$. The values of E_1^{LW} and E_1^{UW} are varied case by case.

The joint's material is fixed and is exactly the isotropic one used for the baseline case UREF ($E = 6.9 \cdot 10^7$ kg/mm $\cdot$ s^2;$\nu = 0.33$). Table 2 presents the analyzed orthotropic configurations. The parameter E_1^r still affects the stability properties: if it is increased, the snap buckling is eventually eliminated (UORTHO5). However, there are important quantitative differences. In fact, as evident from the isotropic configuration's UISO10 response, with a value of $E^r = 2.5 \equiv E_{CR}^r$, buckling instability was avoided. On the contrary, even if the joined wing's geometry, the linear response of point P_1, and the stiffness ratio are kept constant (with respect to UISO10), the orthotropic configuration UORTHO3 (featuring $E_1^r > E_{CR}^r$) presents buckling as seen in Table 2. This suggests that, although E_1^r is related to the physics of the phenomenon (increasing E^r eventually eliminates the instability as seen in Table 2), from a quantitative point of view, it is not the best choice to identify when the instability actually occurs.

Table 2 Cases and relative parameters: details about materials used for different configurations [a]

Case ID	Wing	Young's modulus $E_1 \times 10^{-7}$ kg/mm $\cdot$ s^2	Ratio $E_1^r = E_1^{LW}/E_1^{UW}$	Ratio $A_{22}^r = D_{22}^r = D_{22}^{LW}/D_{22}^{UW}$	Snap
UORTHO1	Upper	5.0	1.8	1.7	Yes
	Lower	8.9			
UORTHO2	Upper	4.5	2.1	1.9	Yes
	Lower	9.5			
UORTHO3	Upper	4.0	2.5	2.2	Yes
	Lower	10.1			
UORTHO4	Upper	3.7	2.8	2.4	Yes
	Lower	10.4			
UORTHO5	Upper	3.4	3.2	2.7	No
	Lower	10.8			

[a]For each case, it holds that $E_2 = E_{REF}$, $\nu = \nu_{REF}$, and $G = G_{REF}$.

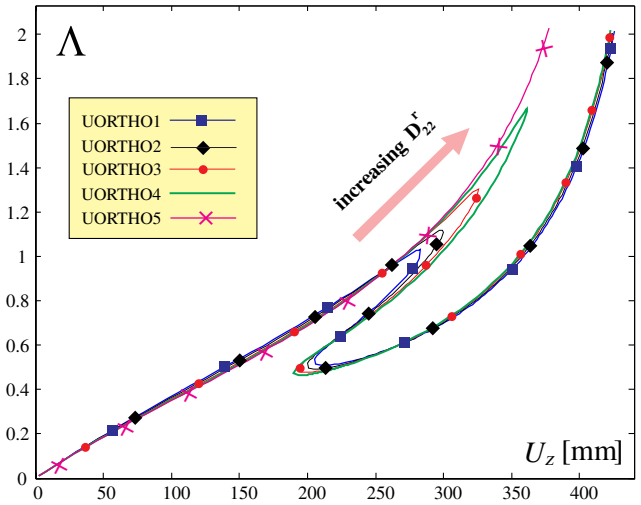

Fig. 4 Load parameter Λ versus cumulative vertical displacement U_z of point P_1 for configurations employing different orthotropic wings. See Table 2 for details.

To find a more representative parameter linked to the stability properties of the system and isolate the driving mechanism, the ratios of extensional and bending stiffnesses are then monitored. These ratios are indicated with A_{mn}^r and D_{mn}^r, respectively. Their explicit definition is as follows:

$$A_{mn}^r = \frac{A_{mn}^{LW}}{A_{mn}^{UW}} \qquad D_{mn}^r = \frac{D_{mn}^{LW}}{D_{mn}^{UW}} \tag{3}$$

where m and n are indices identifying each nonzero term of the corresponding matrix. The superscripts LW and UW indicate that the quantities are referred to the lower wing and upper wing, respectively.

It is observed that each wing is modeled with a single lamina with constant thickness and material properties. This means that matrix $\boldsymbol{A}^r$, which contains the ratios between the extensional stiffnesses, is coincident with matrix $\boldsymbol{D}^r$, which contains the ratios of the bending stiffnesses.

A series of investigations correlates the snap-buckling occurrence with the ratios A_{22}^r and D_{22}^r (see Table 2 and Fig. 4). This is physically expected, since A_{22}^r relates the extensional stiffnesses in the wingspan direction (important, for example, to describe the compression or tension of the wings), whereas D_{22}^r relates the flexural stiffnesses (important in the determination of the principal bending moment of the wings). Moreover, the new critical parameter $[D_{22}^r]_{CR}$ ($[A_{22}^r]_{CR}$) has exactly the same value as the one for the isotropic case E_{CR}^r, giving this a quantitative consistency.

In summary, it has been shown that the snap-buckling disappears when $A_{22}^r = D_{22}^r$ is larger than a critical value. Then, the question is whether A_{22}^r is the actual parameter that needs to be investigated/monitored, if D_{22}^r is the one that needs to be considered, or if both A_{22}^r and D_{22}^r are equally important. The answer represents a crucial concept in the design of a joined wing. For example, if A_{22}^r is the most important term, then the snap buckling is mainly driven by compressive actions. On the other hand, if D_{22}^r is the most important parameter, then the snap buckling occurs mainly because of bending actions. If the two parameters have similar relative importance, the physical mechanism is a combination of both compression and bending.

Since, for a single orthotropic lamina, it is always $A_{22}^r = D_{22}^r$, it is not possible to identify what is physically relevant as far as the instability is concerned unless a larger-than-one number of plies is selected so that it is possible to separately modify $\boldsymbol{A}^r$ and $\boldsymbol{D}^r$ matrices with the consequence that $\boldsymbol{A}^r \neq \boldsymbol{D}^r$.

In particular, several test cases have been introduced with the following assumptions: the lower wing is made of the same isotropic material employed for the reference case; the upper wing is made of a multilayered orthotropic composite laminate with layers made of the

Table 3 Cases and relative parameters: details about materials used for different configurations[a]

Case ID	Wing	Lamination	Ratio $A^r_{22} = A^{LW}_{22}/A^{UW}_{22}$	Ratio $D^r_{22} = D^{LW}_{22}/D^{UW}_{22}$	Snap
UORTHOMP1	Upper	$90_{0.15}/0_{0.7}/90_{0.15}$	2.5	1.3	Yes
UORTHOMP2	Upper	$90_{0.1}/0_{0.35}/90_{0.1}/0_{0.35}/90_{0.1}$	2.5	1.7	Yes
UORTHOMP3	Upper	$90_{0.05}/0_{0.35}/90_{0.2}/0_{0.35}/90_{0.05}$	2.5	2.7	No
UORTHOMP4	Upper	$90_{0.25}/0_{0.5}/90_{0.25}$	1.7	1.0	Yes
UORTHOMP5	Upper	$90_{0.1}/0_{0.25}/90_{0.3}/0_{0.25}/90_{0.1}$	1.7	1.7	Yes
UORTHOMP6	Upper	$90_{0.05}/0_{0.25}/90_{0.4}/0_{0.25}/90_{0.05}$	1.7	2.3	Yes
UORTHOMP7	Upper	$90_{0.03}/0_{0.25}/90_{0.44}/0_{0.25}/90_{0.03}$	1.7	2.9	No
UORTHOMP8	Upper	$90_{0.1}/0_{0.8}/90_{0.1}$	3.4	1.7	Yes
UORTHOMP9	Upper	$90_{0.07}/0_{0.4}/90_{0.06}/0_{0.4}/90_{0.07}$	3.4	2.2	Yes
UORTHOMP10	Upper	$90_{0.05}/0_{0.4}/90_{0.1}/0_{0.4}/90_{0.05}$	3.4	2.8	No

[a]For each case, the lower wing is made of an isotropic material with $E^{LW} = E_{REF}$, $\nu^{LW} = \nu_{REF}$, whereas the upper wing features a composite material with plies laminated as indicated previously. Each ply is manufactured with the same material $E_1 = 8.5 \cdot 10^7$ kg/mm $\cdot$ s^2, $E_2 = 0.66 \cdot 10^7$ kg/mm $\cdot$ s^2, $G_{12} = 0.56 \cdot 10^7$ kg/mm $\cdot$ s^2, and $\nu_{12} = 0.28$.

same material; and the thickness of two generic different layers may be different, but the total thickness of the upper wing is maintained equal to $h = 1$ mm.

Table 3 shows all the analyzed cases and the values of A^r_{22} and D^r_{22} for each configuration. For these cases, a reference closed-form analytical linear solution is impractical to obtain. Thus, the process of constraining the initial slope of the response to a common value, as did for example for the Isotropic case, is not here pursued. However, this does not pose a conceptual limitation.

Figure 5 summarizes the responses of all the performed analyses. As reported in Table 3, it is quite evident that D^r_{22} plays the leading role, since it dictates snap occurrence, where this is not the case for the A^r_{22} parameter. When A^r_{22} is held constant and equal to 1.7, and D^r_{22} is increased from 1.0 to 2.9, the snap buckling disappears. Conversely, if D^r_{22} is held constant and A^r_{22} is varied, the response is not appreciably affected in terms of instability occurrence. Similar considerations, leading to the same conclusions, could be done for the other reported entries of A^r_{22} and D^r_{22}.

The importance of the ratio D^r_{22} is qualitatively consistent with Fig. 6, which shows that, when the snap buckling occurs, a more pronounced inward bending deformation of the upper wing is present compared to cases in which instability is not observed cases. Two configurations are depicted in more detail in Fig. 6: one is associated with the case UORTHO1, which has $E^r_1 = 1.8$ and $D^r_{22} = A^r_{22} = 1.7$; and the other one corresponds to the case UORTHO5, featuring $E^r_1 = 3.2$ and $D^r_{22} = A^r_{22} = 2.7$. Configuration UORTHO1 incurs a snap phenomenon and presents a larger inward bending for the upper wing. It is interesting to observe that,

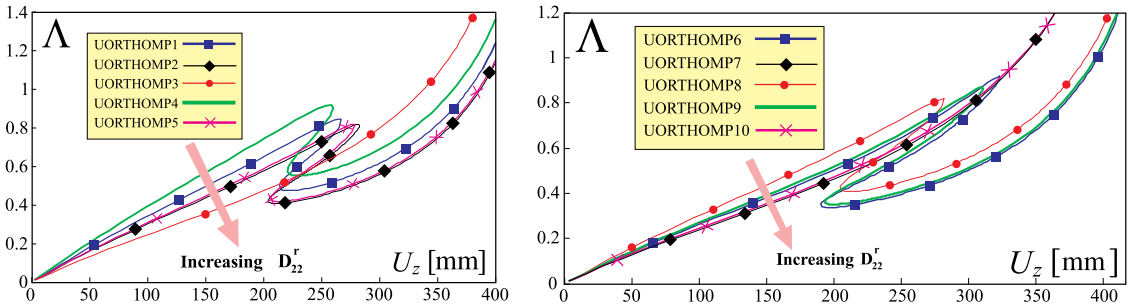

Fig. 5 Responses of different unswept configurations (laminations are indicated in Table 3).

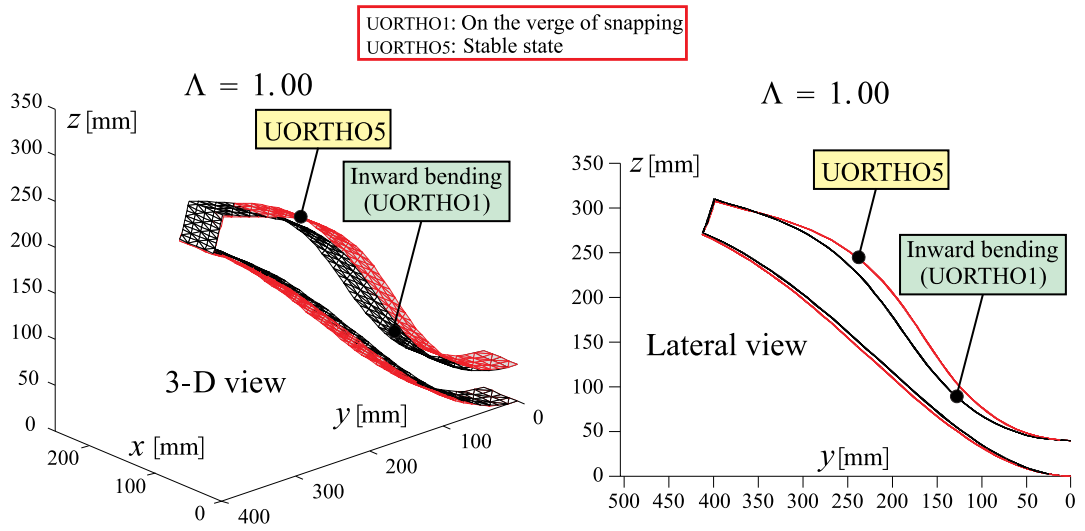

Fig. 6 Comparison of configurations UORTHO1 and UORTHO5 at Λ = 1 (3-D denotes three-dimensional).

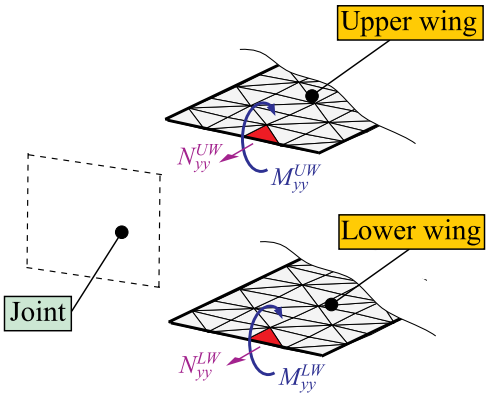

Fig. 7 Wingspan forces (N_{yy}^{UW} and N_{yy}^{LW}) per unit of length and primary bending moments (M_{yy}^{UW} and M_{yy}^{LW}) per unit of length transferred to the upper and lower wings.

both with and without the normalization (prescribed linear displacement of point P_1, adopted for the isotropic and single-lamina orthotropic cases), the critical parameter $[D_{22}^r]_{CR}$ keeps almost the same value (about 2.5).

It should be also observed that the isotropic case investigated in the preceding section and in [32] can be seen as a particularization of the single-lamina orthotropic case investigated here. Thus, the physics ruling the snap-buckling phenomenon is the same. However, in the isotropic case, changing the extensional and bending stiffnesses independently from each other was not possible, and so it was not possible to identify the bending stiffness ratio as the key parameter related to the stability properties of the system.

3. *Joint's Connection and Load Transferring Effects on Snap Buckling*

For both cases of orthotropic and isotropic unswept joined wings, configurations that showed similar tip displacement for the same load level Λ but different nonlinear behavior (i.e., one configuration experienced snap buckling and the other did not; see, for example, Fig. 6) were compared. One of the main features noticed was the different deformation of the upper wing. In particular, the inward bending of the upper wing was more pronounced for the model that was on the verge of snapping. It is true that the curvature distribution of the upper wing depends on all the transmitted force through the joint. However, it is of particular interest to monitor the bending moment M_{yy} transmitted through the joint as a function of the load parameter Λ. More in detail, this is done for the configuration (see Table 1) that is on the verge of snapping (UISO7) and for the configuration (presenting different material properties than the first one but with a similar load-displacement curve up to that load level) that does not present buckling (UISO10) [32]. Figure 7 shows the moment M_{yy} on a finite element on the upper wing and near the joint. Although the interest is toward general behavior more than specific values, to have more reliable predictions, a refined model using approximately 15,000 degrees of freedom (DOF) (against the approximately 2600 DOF of the base model) is used for comparison purposes. These models show an almost perfect agreement in terms of cumulative vertical displacement of point P_1; see Fig. 8. As is well known, the force and moments (see Figs. 9 and 10) converge more slowly when the mesh is refined. The correlation of their trends is

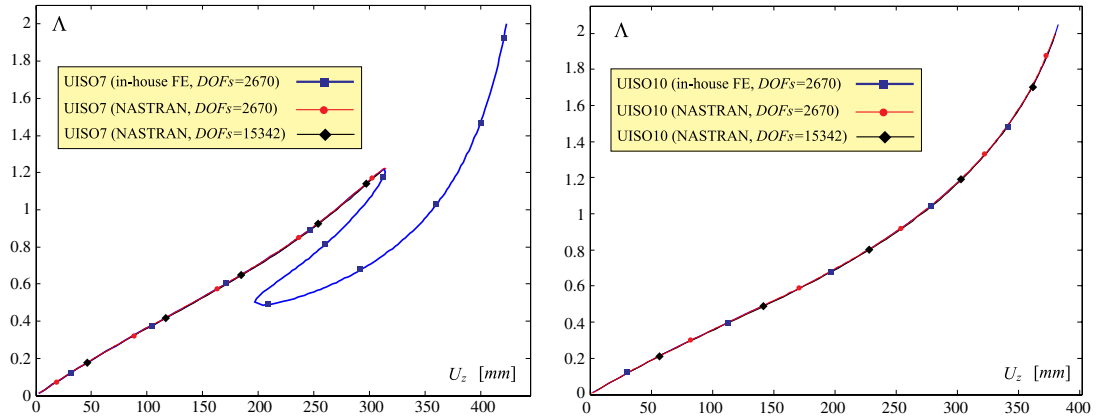

Fig. 8 Response for UISO7 (left) and USIO10 (right) obtained from simulations using different FE solvers and mesh sizes. Both NASTRAN solutions showed convergence issues after the first limit point.

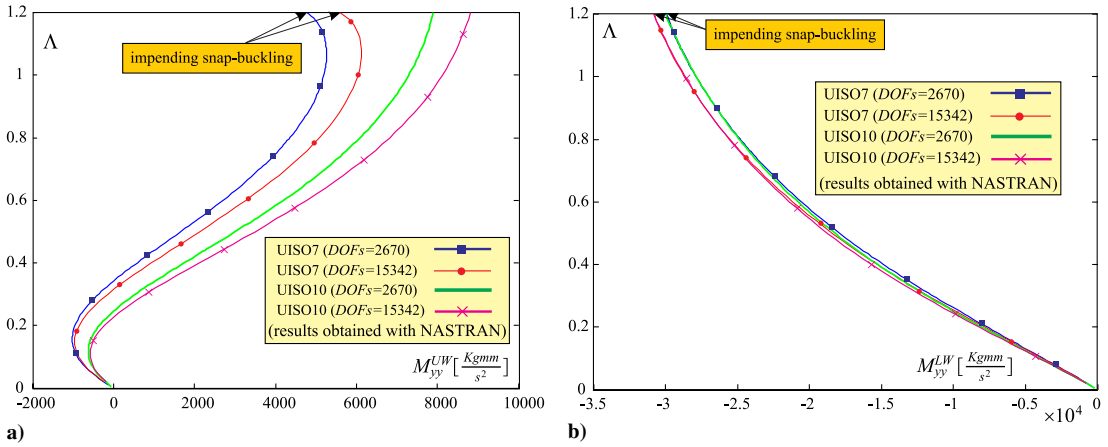

Fig. 9 Bending moment per unit of length M_{yy} for UISO7 and UISO10 cases on the a) upper wing and b) lower wing. See also Fig. 7 for graphical representation.

very good. It should also be pointed out that, since the forces and moments per unit of length are evaluated at the centroid of the elements (see Fig. 7 for the base model), a refining of the mesh implies a calculation of these quantities on a different (but close) point. The interest of this discussion is to show the trends. Thus, this fact does not affect the following discussion.

In Fig. 9, the value of M_{yy} is plotted for both the upper and lower wings for both cases. Considering the upper wing, it is possible to observe that M_{yy}^{UW} shows a similar trend in the prebuckling area. However, the configuration that does not experience snap buckling (UISO10) presents a larger moment M_{yy}^{UW} compared to the one corresponding to UISO7. At a certain load parameter, smaller than the critical value, the moment relative to configuration UISO7 starts diminishing in value, and eventually, the snap buckling occurs. For the lower wing, the bending moments of the UISO7 and UISO10 configurations are practically identical.

For completeness, Fig. 10 shows the force per unit of length N_{yy} on the upper wing (see also Fig. 7).

The different trends regarding the transmitted bending moment (see Fig. 9a) suggest that the snap-buckling occurrence could be strictly tied with M_{yy}. To further demonstrate this observation, the boundary conditions between the joint and the upper (or lower) wings are now modified to reduce the amount of moment that is transferred. This is accomplished by the adoption of a multifreedom constraint which allows the joint-upper-wing or joint-lower-wing relative rotation. To simulate some stiffness of the joint, a relatively small torsional spring ($k_\vartheta = 100\ (\mathrm{kg}\cdot\mathrm{mm}^2)/(\mathrm{s}^2\cdot\mathrm{rad})$) has also been added at the joint–wing connection. It should be noted that a large value for the spring stiffness would correspond to a perfect joint's connection of the types analyzed so far, whereas a zero value for the stiffness of the spring would correspond to a perfect hinge connection. Since the adopted value for the torsional stiffness is quite small compared to the stiffness of the finite elements, the simulated joint–wing connection is similar (but not equivalent) to a hinge connection. This set of boundary conditions is referred to as a quasi-hinge connection in this work.

A quasi-hinge connection reduces the amount of moment transferred by the joint to the wing. Thus, it is expected that this connection has the tendency to reduce or eliminate the buckling occurrence. To prove that, three configurations based on UREF are considered: one with perfect joints, one with a quasi-hinge connection between the joint and upper wing, and one with a quasi-hinge connection between the joint and the lower wing. The related nonlinear responses are plotted in Fig. 11. It can be observed that the snap buckling disappears in both cases in which a quasi-hinge connection is employed. Moreover, reducing the bending moment transmission prevents the snap from occurring. Moreover, if the responses relative to these cases are superimposed, it is possible to realize that the precritical states for the perfect joint case show a larger value of the stiffness (i.e., higher slope of the displacement-load curve in Fig. 11). Thus, the configurations featuring a quasi-hinge connection experience a reduction of stiffness, which is more pronounced when the quasi-hinge connection is located between the joint and the upper wing. In summary, the presented analyses lead to the conclusion that bending action transmission is one of the main sources of nonlinearities when stability is concerned. When the perfect joint is considered, the stiffness of the system is first increased, but eventually, the instability phenomenon occurs (see Fig. 11). When the bending moment is partially transmitted, the response does not present any snap-buckling phenomena. However, there is a consistent loss of stiffness (see Fig. 11).

Studies on the connection between wings have already been undertaken: for example, by Stearman et al. [29]. In that work, the rigid connection was assessed as being the most favorable in terms of root bending moment alleviation and stiffness. And, at least from a stiffness perspective, the results are in agreement with the results presented in the current work. However, the analyses of [29] were obtained with linear models; thus, phenomena such as snap buckling could not have been predicted or included. Furthermore, it should be noted that the conclusions apply for the particular configuration (a Sensorcraft/joined-wing one) and load condition. The highly complex structural response of the joined wings needs careful case-by-case investigation.

The authors would also like to quote a passage from [29], in which it is stated that the overconstrained nature of the system could give rise to significant load transfer through the joint that could be detrimental to the structural stability of the system: to properly take them into account a nonlinear analysis may be necessary. The present findings (see Figs. 11 and 12) confirm this importance: the bending moment transfer has a primary role in snap-buckling occurrence.

4. *Composite Materials (Anisotropic Case)*

Previous discussions showed that, for the isotropic and orthotropic cases, the driving mechanism that leads to the snap buckling is closely tied with bending effects. It was also demonstrated that the bending stiffness ratio D_{22}^r was an effective parameter to predict if the nonlinear response presents a snap-buckling instability. In particular, it was shown that the upper wing has to be more bending-compliant to avoid the snap buckling. It was found that, when $D_{22}^r \equiv D_{22}^{\mathrm{LW}}/D_{22}^{\mathrm{UW}}$ is bigger than a critical value, then the instability disappears; $[D_{22}^r]_{\mathrm{CR}}$ does not represent a universal value; on the contrary, its magnitude is expected to be a case-dependent parameter.

For the same unswept joined-wing layout, the next step is the adoption of composite materials to introduce anisotropic effects and investigate how they influence the nonlinear response. In particular, two main questions are here answered. Is D_{22}^r sufficient to describe the tendency of the structure to experience a snap buckling? What are

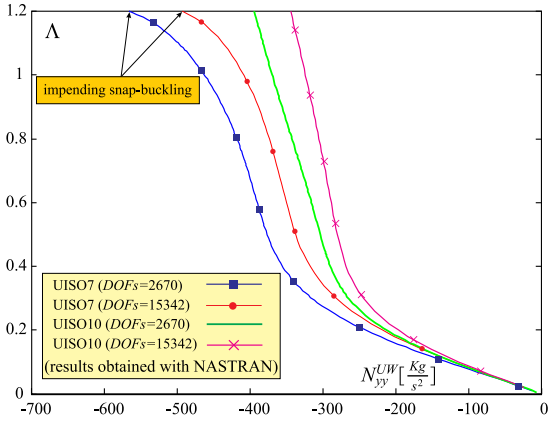

Fig. 10 In-plane force per unit of length N_{yy} on the upper wing for UISO7 and UISO10 cases.

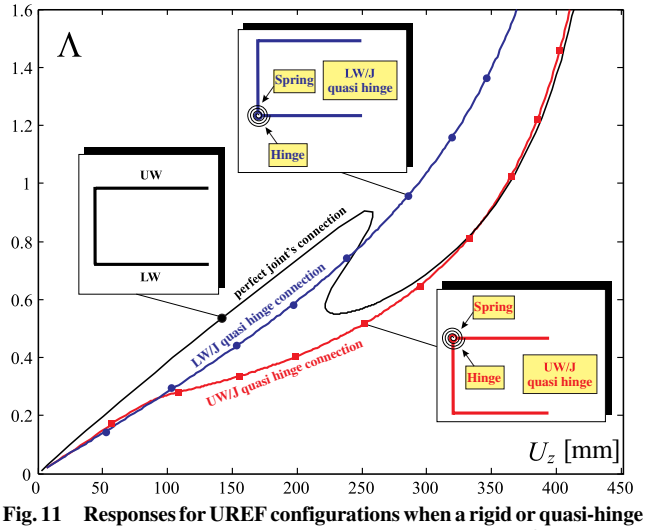

Fig. 11 Responses for UREF configurations when a rigid or quasi-hinge connection is used between the joint and the upper (UW/*J*) or lower (LW/*J*) wing.

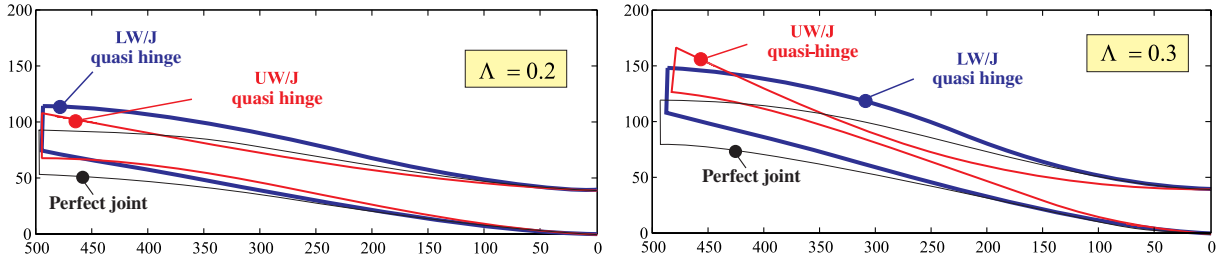

Fig. 12 Comparison of deformed structures for different (Λ) values for the perfect and quasi-hinge connection cases.

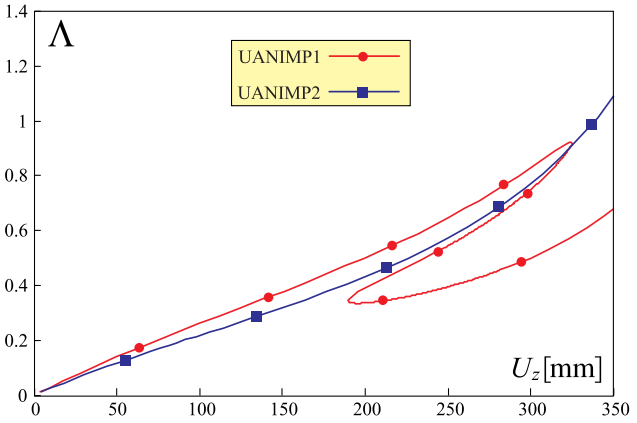

Fig. 13 Responses for configurations UANIMP1 and UANIMP2. See Table 4 for details.

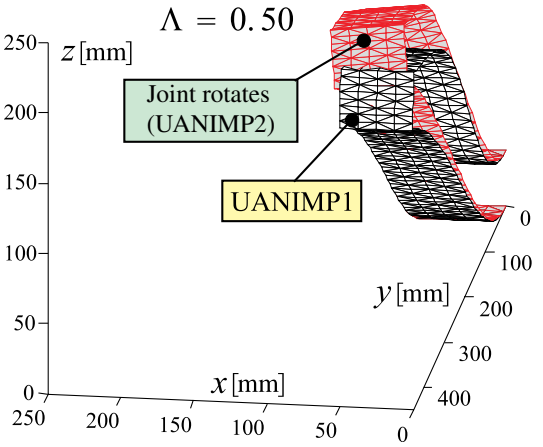

Fig. 14 Comparison of deformed configurations for configurations UANIMP1 and UANIMP2.

the effects of anisotropy on the global bending stiffness and snap buckling?

To answer the first question, two new configurations are investigated (see Table 4). In the first one, named UANIMP1, the lower wing is isotropic and the material is the one adopted for the UREF configuration. The upper wing is simulated with a multilayered orthotropic plate. The second configuration, named UANIMP2, presents a symmetric laminate for the upper wing, whereas the lower wing is made of the same isotropic reference material. Both configurations present the same value for D_{22}^r; however, the nonlinear responses are dramatically different (see Fig. 13) and configuration UANIMP2 does not experience snap buckling. This qualitative investigation shows that the new coupling between the torsional deformation and bending moment plays an important role as far as the stability properties are concerned.

Figure 14 shows how the anisotropy introduces torsional deformations (configuration UANIMP2) that are not present for configuration UANIMP1. A series of additional configurations have been created (see Table 5 and Fig. 15). The lower wing is isotropic, and the adopted material is the one used for the UREF case. The upper wing is simulated with a single lamina for which the orientation is varied according to Table 5. Results indicate (see Fig. 16 and Table 5) that the bending–torsional coupling has a major role in determining when the snap buckling occurs. This is clearly understood if, for example, configurations UANISP2 and UANISP4 are compared. The two configurations do not present snap buckling; although this was expected for the first one having $D_{22}^r > [D_{22}^r]_{\mathrm{CR}}$, it was not expected for the second one, for which $D_{22}^r < [D_{22}^r]_{\mathrm{CR}}$. Similar situation arises when comparing UANISP11 and UANISP12. Unexpectedly behaving cases present a value of D_{26}^{UW} different than zero. Since the wing system is unswept, the coupling between the torsion and bending are due only to the anisotropy of the material.

This is why, for the anisotropic case, understanding the mechanism that leads to the instability is more challenging.

To answer the second question (i.e., identify what are the effects of the anisotropy on global bending stiffness and snap buckling), three different configurations (UANISP15, UANISP4, and UANISP12 [see Table 5]) are selected. None of them experiences the nonlinear buckling, and, according to Fig. 17, they present high overall stiffness. The configurations UANISP4 and UANISP12 are stiffer than the configuration UANISP15 (especially for larger values of the load step Λ), confirming that composite materials can be effectively used to change the structural behavior of the system.

In practice, the design is more challenging since it must take into account the structural weight and stress levels. Moreover, the actual aerodynamic loads are of a nonconservative type and the torsional–bending coupling is then even more important: the aerodynamic forces are heavily affected by a change of angle of attack (torsion) of the wing. This study is the first step in the understanding of the difficulties and challenges associated with the nonlinear response for the case of anisotropic joined wings.

Table 4 Cases and relative parameters: details about materials used for different configurations[a]

Case ID	Wing	Lamination	Ratio $D_{22}^r = D_{22}^{\mathrm{LW}}/D_{22}^{\mathrm{UW}}$	Snap
UANIMP1	Upper	$90_{0.049}/0_{0.25}/90_{0.402}/0_{0.25}/90_{0.049}$	2.4	Yes
UANIMP2	Upper	$17_{0.1}/45_{0.8}/17_{0.1}$	2.4	No

[a]For each case, the lower wing is composed of the reference isotropic material, where the upper wing is composed of a composite material with the same material: $E_1 = 8.5 \cdot 10^7$ kg/mm · s^2, $E_2 = 0.66 \cdot 10^7$ kg/mm · s^2, $G_{12} = 2.6 \cdot 10^7$ kg/mm · s^2, and $\nu_{12} = 0.33$.

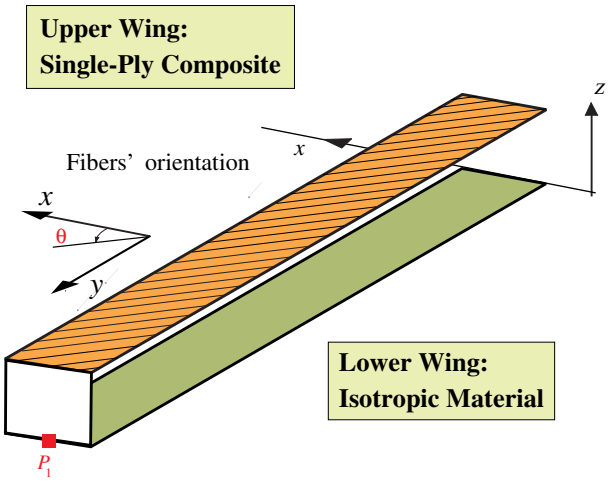

Fig. 15 Unswept configurations for anisotropic cases.

VI. Swept Joined Wings and Composites

From the analysis of unswept joined wings, two main concepts could be identified. First, the ratio between the bending stiffness of the wings is an important parameter to establish if the snap buckling occurs. In particular, the upper wing has to be more bending-compliant than the lower wing to remove the instability.

Second, the anisotropy introduces a coupling between the torsion and bending that is not present in an isotropic unswept joined wing. This coupling modifies the snap-buckling occurrence.

A similar study is now attempted for the swept joined wings (see Fig. 2). It is necessary to investigate this case since, even when isotropic materials are used, a coupling between the bending and torsion due to the geometry of the wing system arises. It may also be observed (see Fig. 2) that the sweep angle is moderately low. It is then reasonable to expect that the snap occurrence is still regulated by bending-stiffness-related parameters.

To better investigate the physics related to the bending, it is useful to introduce two local coordinate systems: one for each wing. The direction of the z axis remains parallel to the global z axis, whereas the local y axis runs along the wingspan direction. In such a way, the terms of the D matrices for the upper and lower wings maintain an immediate physical interpretation. Figure 2 clarifies the orientation of the lower- and upper-wing local axes.

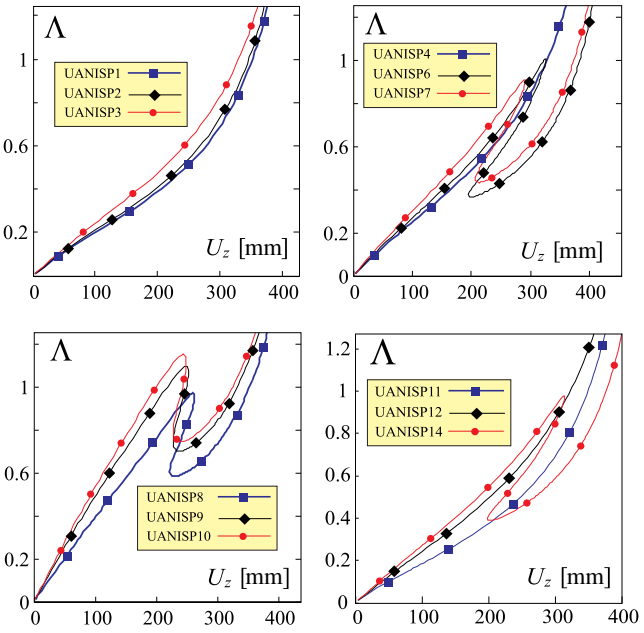

Fig. 16 Responses for different unswept configurations featuring a single layer composite upper wing. See Table 5 for details.

A. Effects of Lower-to-Upper-Wing Stiffness Ratio

1. *Isotropic Case*

The ratio of the Young's moduli of the two wings is varied. However, Young's moduli are selected so that the initial slopes of the displacements are the same (the initial slope is related to the stiffness of the linear analysis). The details about the materials of each configuration are shown in Table 6 and Fig. 18, and the graphs of the cumulative vertical displacement of point P_1 are presented in Fig. 19. It can be inferred that, as in the unswept case, the ratio $E^r = E^{\mathrm{LW}}/E^{\mathrm{UW}}$ has an important role. However, the required value for avoiding snap is considerably larger (see Table 6) than the one needed for the unswept wing case (see Table 1). This means that the lower wing has to be much stiffer than the upper wing in order to avoid snap buckling.

It is possible to observe that each wing of the swept configuration is slightly longer and leaner (higher aspect ratio) than the previous unswept cases. However, since the sweep angle is small, the aspect

Table 5 Cases and relative parameters: details about materials used for different configurations[a]

Case ID	Wing	Orientation	Ratio $D^r_{22} = D^{\mathrm{LW}}_{22}/D^{\mathrm{UW}}_{22}$	$D^{\mathrm{UW}}_{26} \times 10^{-7}$, kg/mm · s^2	Snap	UW Data
UANISP1	Upper	0 deg	4.5	0	No	
UANISP2	Upper	15 deg	3.4	0.09	No	
UANISP3	Upper	30 deg	1.9	0.18	No	
UANISP4	Upper	32.5 deg	1.8	0.19	No	$E_1 = 12.5$
UANISP5	Upper	35 deg	1.6	0.20	Yes	$E_2 = 1.7$
UANISP6	Upper	37.5 deg	1.5	0.21	Yes	$G_{12} = 2.7$
UANISP7	Upper	45 deg	1.2	0.23	Yes	$\nu_{12} = 0.33$
UANISP8	Upper	60 deg	0.8	0.22	Yes	
UANISP9	Upper	75 deg	0.7	0.14	Yes	
UANISP10	Upper	90 deg	0.6	0	Yes	
UANISP11	Upper	45 deg	2.6	0.16	No	$E_1 = 8.5$
UANISP12	Upper	60 deg	1.4	0.20	No	$E_2 = 0.66$
UANISP13	Upper	62.5 deg	1.3	0.20	Yes	$G_{12} = 0.56$
UANISP14	Upper	65 deg	1.3	0.19	Yes	$\nu_{12} = 0.28$
UANISP15	Upper	Isotropic	2.6	0	No	$E = 2.65$ $\nu = 0.33$

[a]For each case, the lower wing is made of reference isotropic material, where the upper wing is composed of a single ply with fibers oriented as indicate previously (cases UANISP1 through UANISP14) or of an isotropic material (UANISP15). The Young and shear moduli of this Table are expressed in kg/mm · s^2, and the values reported in the table need to be multiplied by 10^7.

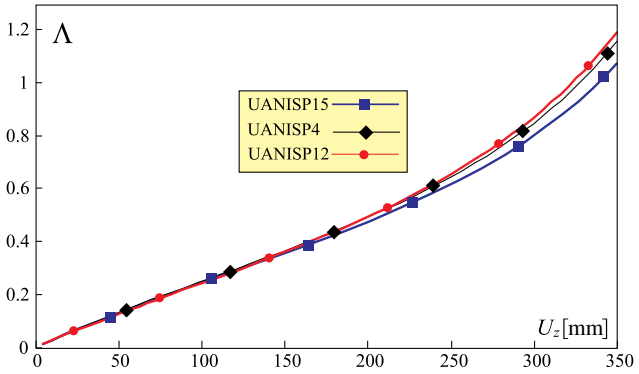

Fig. 17 Responses for UANISP4, UANISP12 and UANISP15 configurations. See Table 5 for details.

ratio is not significantly affected. The consistent difference of the critical ratio E^r found for the swept case could be thought to come mainly from effects introduced by the torsion.

Analyses of two configurations [32] (one incurring in snap, SISO5; and one not, SISO8) for two different load conditions are depicted in Figs. 20 and 21. For the load level $\Lambda = 0.5$, SISO5 is not very far to buckle; however, the two deformed shapes are almost superimposed (see Fig. 20), except for the upper wings. In the SISO5 case, the upper wing experiences a more pronounced inward bending deformation, similar with what was found for the swept cases.

The load level $\Lambda = 0.6$ represents a postbuckling situation for the configuration SISO5, as it could be verified in Fig. 19b. Besides experiencing an almost rigid rotation along the x axis, in this case, the joint undergoes a negative rotation along the global y axis as well (see Fig. 21).

In conclusion, the interactions between the wings are more complicated in the case of swept joined wings, even when isotropic materials are used. This is due to the rise of forces inherent to the geometrical layout, which couples the bending and torsional effects. These forces have an important role in influencing the snap phenomenon: although the spanwise bending actions drive the instability phenomenon, torsion contributes to regulate it. For example, compared to the unswept isotropic cases, the lower wing has to be significantly stiffer in order for snap to be avoided. This could be intuitively explained as follows: Figure 21 shows that, when the instability takes place, a significant rigid rotation of the joint is experienced (SISO5 configuration). Thus, the high stiffness is "required" to also counteract this joint's rotation, and thus to avoid the snap bucking.

Table 6 Cases and relative parameters: details about isotropic materials used for different swept joined wings (Poisson ratio is $\nu = 0.33$ for each case)

Case ID	Wing	Young's modulus $E \times 10^{-7}$, kg/mm · s^2	Ratio $E^r = E^{LW}/E^{UW}$	Snap
SREF	Upper	6.9	1	Yes
	Lower	6.9		
SISO1	Upper	12	0.2	Yes
	Lower	2.5		
SISO2	Upper	5	1.8	Yes
	Lower	8.9		
SISO3	Upper	4	2.5	Yes
	Lower	10.1		
SISO4	Upper	3	3.8	Yes
	Lower	11.3		
SISO5	Upper	2.5	4.8	Yes
	Lower	12.0		
SISO6	Upper	2.2	5.6	Yes
	Lower	12.4		
SISO7	Upper	2.1	6.0	Yes
	Lower	12.5		
SISO8	Upper	2.0	6.3	No
	Lower	12.6		

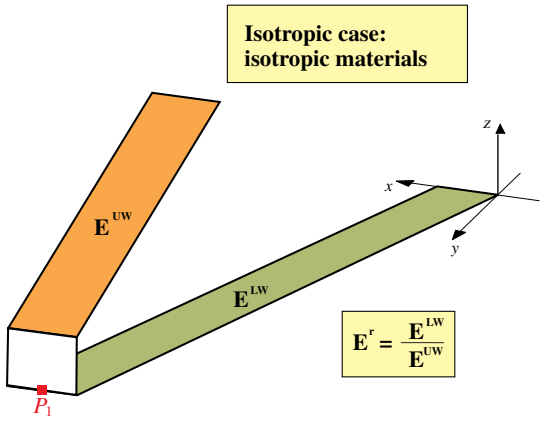

Fig. 18 Swept configurations for isotropic cases and definition of lower-to-upper wing stiffness ratio.

2. Orthotropic Cases

The introduction of an orthotropic material for the wings allows not only the differentiation between the relative importance of the Young's moduli E_1 and E_2, but it also gives the valuable possibility to isolate and study more in depth the torsional effects. This was not possible for unswept layouts since, featuring the configuration geometrical symmetry, no torsional effects were introduced in the structure.

The stiffness parameter D_{66} is now varied to explore the effects due to the torsion, but the bending stiffness ratio, extensively discussed in the preceding sections, is not modified. The use of orthotropic material gives the possibility to act on the D_{66} coefficient, maintaining the same bending stiffness ratio. In fact, as could be inferred from its well-known definition, the D_{66} parameter could be fine-tuned through the adoption of different values of the material's shear modulus G_{12}. Moreover, this last material property does not influence the remaining parameters of the stiffness matrix D. It is thus straightforward to selectively evaluate the importance of torsional deformation on the system response.

In this regard, SREF is chosen as the starting configuration. Then, for each wing, the Young's moduli and Poisson's ratio are set such that

$$E_1^{UW} = E_2^{UW} = E_1^{LW} = E_2^{LW} = E_{REF} \tag{4}$$

$$\nu_{12}^{UW} = \nu_{12}^{LW} = \nu_{REF} \tag{5}$$

Different values of G_{12}^{UW} and G_{12}^{UW} are chosen, with a direct effect on D_{66}^{UW} and D_{66}^{LW}, respectively, as shown in Table 7 and Fig. 22. The responses are depicted in Fig. 23. It could be inferred that torsional stiffness has an important effect on the behavior of the system. If it is increased, torsional deformations are smaller; thus, ideally, the response is expected to be qualitatively similar to the one of the unswept case (with isotropic or orthotropic wings). This is supported, noticing that the SORTHO cases' responses are qualitatively similar to the UREF's (see [32]), showing a more abrupt snap-buckling occurrence; that is, the instability occurs without a progressive previous loss of stiffness.

As could be seen in Fig. 23, if torsional stiffness is increased, to a certain extent, no instability phenomenon occurs, which is different than the unswept case where it was not possible to eliminate buckling when $D_{22}^r < [D_{22}^r]_{CR}$. This difference is a consequence of the structure's layout and overconstrained nature of the system. In practice, in cases such as SORTHO5, the torsional stiffness has a dominant role on the bending mode through the geometrical coupling, and this interaction limits the pertinence of considering the similarity between the swept and unswept cases.

In summary, in this particular overconstrained system in which bending and torsion are also coupled as a consequence of the sweep angle, it is very difficult to separate the effects on the structural response driven by one or the other deformation.

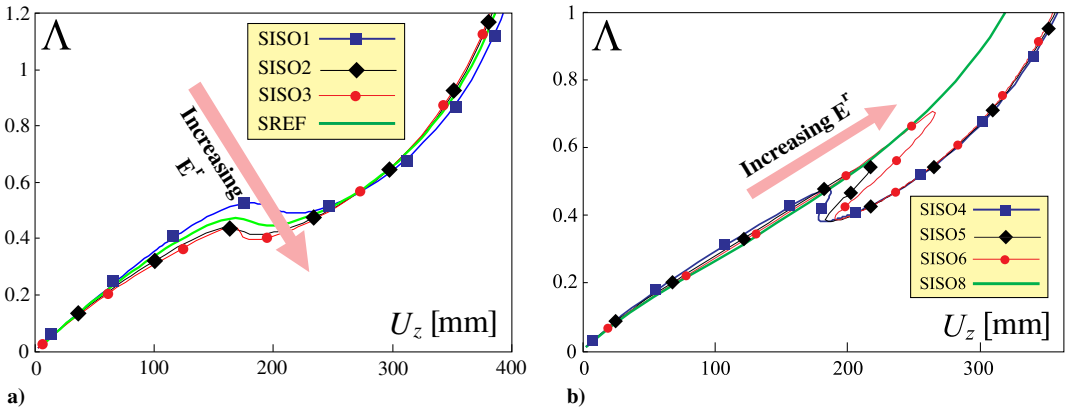

Fig. 19 Responses for different swept configurations featuring isotropic materials. See Table 6 for details.

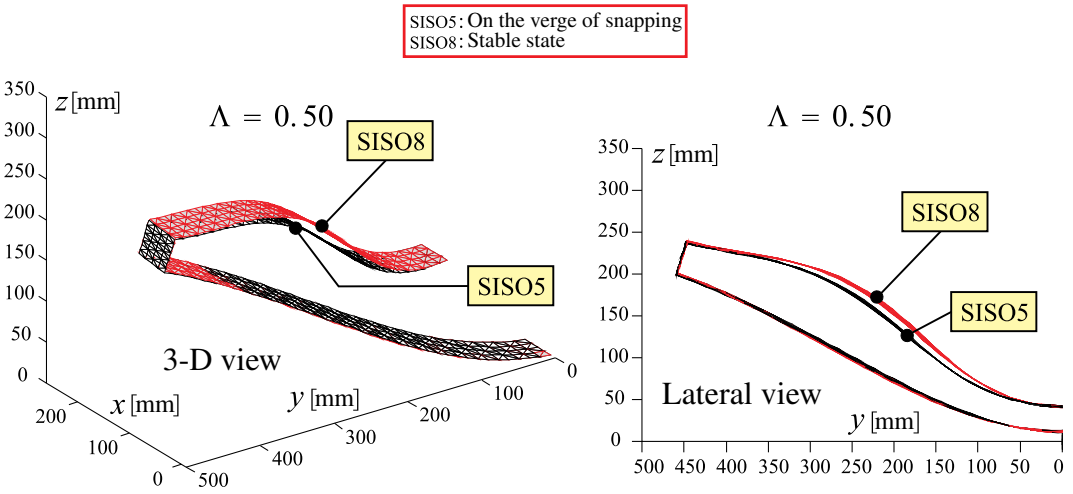

Fig. 20 Comparison of deformed configurations SISO5 and SISO8 at Λ = 0.5: tridimensional and side views.

3. Anisotropic Effects

In this section, the lower wing is assumed to be made of the same isotropic material used for the UREF configuration. However, the upper wing is now composed of a single lamina. The fibers' orientation is measured starting from the upper-wing local axis x^{UW}, as depicted in Figs. 2 and 24. Table 8 reports the configurations used to assess the anisotropic effects for the swept joined wing. It may be inferred that the influence of torsion is now of primary importance. In

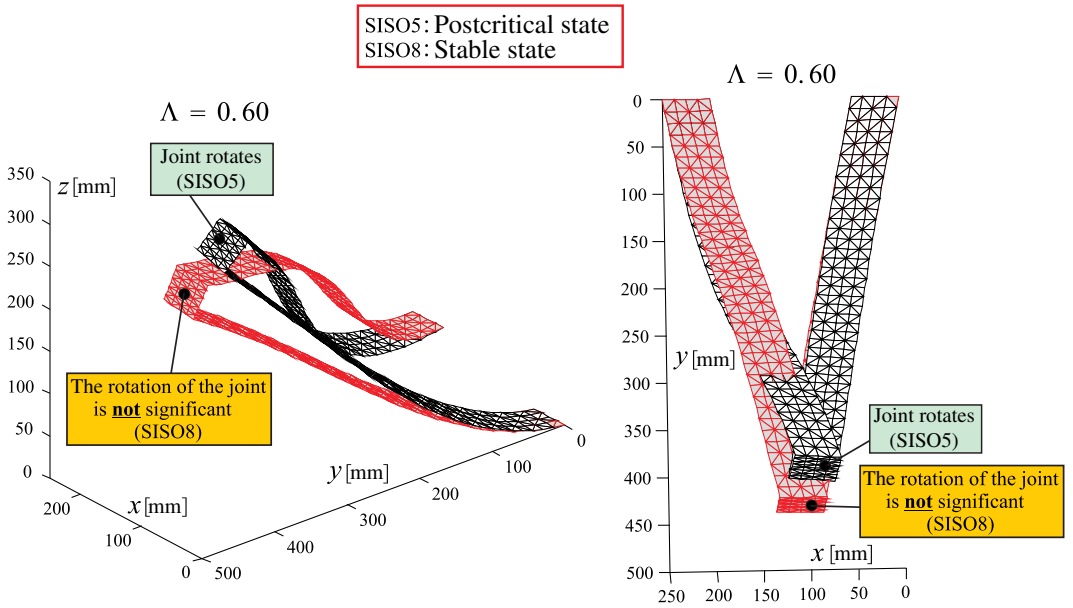

Fig. 21 Comparison of configurations SISO5 and SISO8 at Λ = 0.6: tridimensional and upper views. SISO5 is in its postsnap configuration.

Table 7 Cases and relative parameters: details about orthotropic materials used for different swept joined wings[a]

Case ID	Wing	Shear modulus $G_{12} \times 10^{-7}$, kg/mm · s^2	Ratio $E_1^r = E_1^{LW}/E_1^{UW}$	Snap
SREF	Upper	2.6	1	Yes
	Lower	2.6		
SORTHO1	Upper	120	1	Yes
	Lower	120		
SORTHO2	Upper	300	1	Yes
	Lower	300		
SORTHO3	Upper	600	1	Yes
	Lower	600		
SORTHO4	Upper	1500	1	Yes
	Lower	1500		
SORTHO5	Upper	2500	1	No
	Lower	2500		

[a]The Young's moduli and Poisson ratio are $E_1 = E_2 = E_{REF}$ and $\nu_{12} = \nu_{REF}$ for each wing in all cases. Thus, every considered configuration has the ratio D_{22}^r equal to 1.

fact, some configurations featuring a relatively small value of D_{22}^r do not present any snap-buckling phenomena. It is relevant to investigate the effect of the sign for D_{26}^{UW} for practically unchanged D_{22}^r parameters. For example, configuration SANISP16 (for which $D_{22}^r = 1.39$ and $D_{26}^{UW} = -0.20$ kg · mm^2/s^2) does not experience buckling, whereas configuration SANISP6 (for which $D_{22}^r = 1.30$ and $D_{26}^{UW} = +0.20$ kg · mm^2/s^2) does experience instability.

Not all of the configurations reported in Table 8 experience buckling. It is then of a practical importance to identify the conditions for which buckling occurs from a graphical point of view. In particular, the so-called snap-buckling region (SBR) for joined wings [27] can be seen in Fig. 25. It should be noted that the SBR is actually the union of two subregions that do not present symmetry with respect to the zero angle. This is expected. since the joined wing and its materials do not present symmetries and the complex bending–torsion coupling affects the nonlinear response in a nontrivial manner.

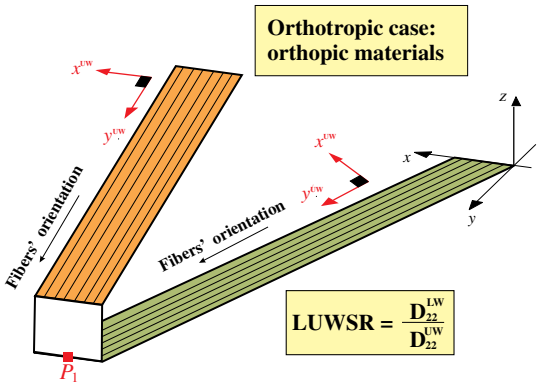

Fig. 22 Swept configurations for orthotropic cases and definition of lower-to-upper wing stiffness ratio (LUWSR).

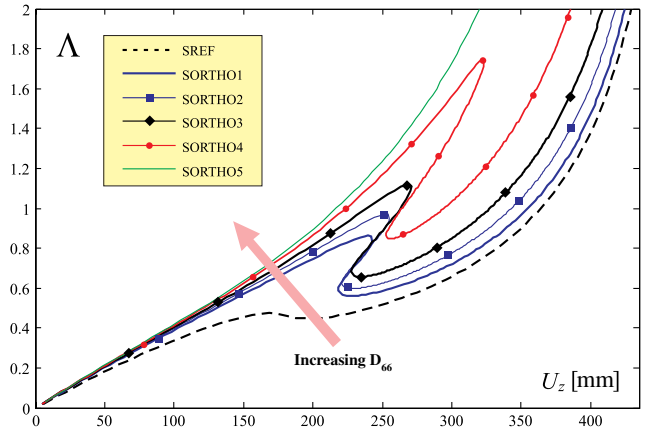

Fig. 23 Responses for different swept configurations featuring orthotropic materials. See Table 7 for details.

Figure 26 shows the responses relative to some of the cases reported in Table 8.

Figure 27 graphically shows the connection between typical responses and the fibers' orientation. Some observations could be stated. When the fibers are directed along the upper wing's chordwise direction (local x axis), the response is not very stiff and snap buckling does not occur. This is not surprising, since the lower-to-upper wing bending stiffness ratio has a large value (see, for example, configuration SANISP1 in Table 8: D_{22}^r is 10.71). It is also expected that, if the fibers are rotated, the structure exhibits (overall) a stiffer response, since material is properly oriented to counteract the flexional actions. However, this is not always the case. If the fibers are rotated in the positive ϑ direction, the response is much stiffer (see, for example, SANISP3 in Fig. 27), whereas if they are rotated in the opposite direction, the response does not only contradict the intuition based on a stiffness perspective but, with a further decrease of ϑ, a snap phenomenon occurs (see SANISP12, SANISP18, and SANISP8 in Fig. 27). It is not trivial to interpret and fully understand this behavior. The bending–torsion coupling at both geometrical and material levels for these cases is unfavorable, and it gives rise to configurations that are compliant in resisting the load, and could even undergo instability.

With a further decrease of ϑ, an interesting behavior is detected. Comparing SANISP18 and SANISP8, both having buckling problems, and a main difference is observed: SANISP18 corresponds to an abrupt buckling, whereas SANISP8 has a mild snap; that is, in the whole neighborhood of the limit point, there is loss in stiffness. If the fibers' orientation is decreased to the point that buckling disappears (as, for example, happens with configuration SANISP16), this local softening is still observed.

Notice that the initial response has not significantly changed from the SANISP1 case, although the fibers' orientation has varied by 50 deg.

The pattern showin in SANISP16 is maintained if the angle is further decreased. But, the structural response progressively gains stiffness until the fibers are oriented approximately along the spanwise direction (SANISP10). Based on the previously gained experience about the stiffness ratio influence on snap occurrence, it is unexpected that this configuration does not show a snap-buckling phenomenon, although the local loss of stiffness pattern is practically as inconvenient as an instability.

If starting from $\vartheta = 0$ deg, the angle is increased the responses follow an expected behavior. In fact, stiffness of the response increases (SANISP3) and snap buckling eventually occurs (SANISP4). Notice that this snap has the usual behavior, with the limit point occurring without having any loss of stiffness in the load-displacement curve preceding the limit point. Now, a further increase

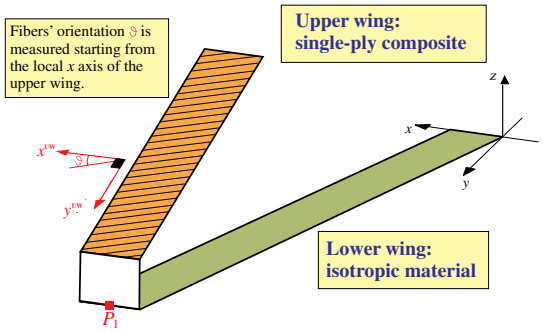

Fig. 24 Swept configurations for anisotropic cases.

Table 8 Cases and relative parameters: test cases[a]

Case ID	Wing	Orientation: angle measured from x^{UW}; x, deg	Ratio $D^r_{22} = D^{LW}_{22}/D^{UW}_{22}$	$D^{UW}_{26} \times 10^{-7}$, kg · mm^2/s^2	Snap
SANISP1	Upper	−11.3 (0)	10.71	−0.01	No
SANISP2	Upper	33.7 (45)	4.60	0.10	No
SANISP3	Upper	48.7 (60)	2.22	0.18	No
SANISP4	Upper	53.7 (65)	1.80	0.20	Yes
SANISP5	Upper	58.7 (70)	1.51	0.20	Yes
SANISP6	Upper	63.7 (75)	1.30	0.20	Yes
SANISP7	Upper	78.7 (90)	0.97	0.11	Yes
SANISP8	Upper	−56.3 (−45)	1.64	−0.20	Yes
SANISP9	Upper	−86.3 (−75)	0.91	−0.04	No
SANISP10	Upper	88.7 (−80)	0.91	0.01	No
SANISP11	Upper	83.7 (−85)	0.92	0.07	Yes
SANISP12	Upper	−41.3 (−30)	3.13	−0.15	No
SANISP13	Upper	−71.3 (−60)	1.09	−0.17	No
SANISP14	Upper	73.7 (85)	1.04	0.15	Yes
SANISP15	Upper	−66.3 (−55)	1.21	−0.19	No
SANISP16	Upper	−61.3 (−50)	1.39	−0.20	No
SANISP17	Upper	−51.3 (−40)	1.99	−0.19	Yes
SANISP18	Upper	−46.3 (−35)	2.47	−0.17	Yes

[a]For each case, the lower wing is made of the reference isotropic material, whereas the upper wing is a single ply. The material used for the upper wing presents $E^{UW}_1 = 8.5 \cdot 10^7$ kg · mm^2/s^2, $E^{UW}_2 = 0.66 \cdot 10^7$ kg · mm^2/s^2, $G^{UW}_{12} = 0.56 \cdot 10^7$ kg · mm^2/s^2, and $\nu^{UW}_{12} = 0.28$. The fibers' angle is measured starting from the upper wing's local coordinate system x^{UW}. In parentheses, the same fiber's angle is referred to as the global coordinate system x axis (see Fig. 25).

in the fibers' angle leads to an initial increase in stiffness, followed, however, by n snap-buckling instability at a lower load level. The instability is characterized now (see SANISP11) by a local softening in the limit point region (mild snap buckling), similar to what is observed for the SANISP8 configuration.

Unexpectedly, a further increase in ϑ leads to a response not showing a snap-buckling phenomena, but the local softening is still present (SANISP10).

In summary, starting from $\vartheta = 0$, if the angle is changed in the positive direction, the response becomes stiffer and snap-buckling occurs. Then, due probably to torsional effects, local softening is introduced in the neighborhood of the limit point region. If the angle is changed in the negative direction, the response experiences instability without being initially stiffer. In this case, the bending–torsion coupling counteracts the typically stiffer behavior related with smaller D^r_{22} (and same D^{LW}_{22}), but it does not avoid snap occurrence. Finally, when the fibers are oriented nearly along the spanwise direction, no instability is present, although there is a pronounced loss of stiffness.

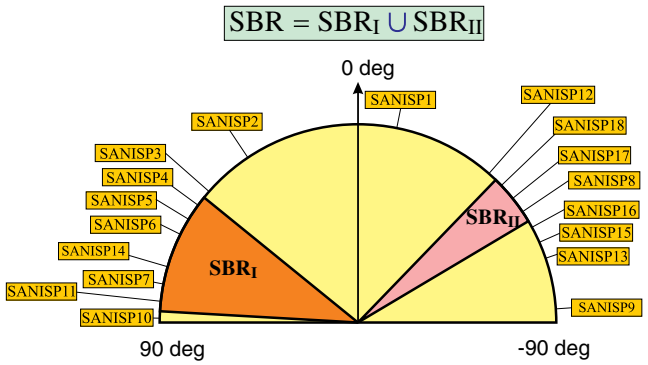

Fig. 25 Snap-buckling region for configurations with different orientations of the upper wing's fibers. The configurations in the SBR experience buckling.

It is the authors' opinion that further studies are needed in order to better understand the phenomenon at its basic level. In fact, although in this case the structural response is basically regulated by the bending–torsion coupling, the strong nonlinear behavior represents an added complication and makes extremely difficult, and possibly unsuccessful, the attempt to explain in detail the essence of the problem, breaking it down in simpler cases.

B. Joint's Height Effects in the Case of Anisotropic Swept Joined Wings

In [27], it was demonstrated that, for the case of isotropic materials, the increase of the height of the joint was beneficial. This is confirmed in this work for the case of composite materials, as clearly shown in Fig. 28, where SANISP4 and SANISP11 (see also Table 8) are presented. A joint's height larger than a certain value ($b = 65/50a$ and $b = 50/50a$ for the cases of Figs. 28a and 28b, respectively) leads to a stiffer snap-buckling-free response. This is the concept of the upper-limit snap-buckling region introduced in [27] for the isotropic case.

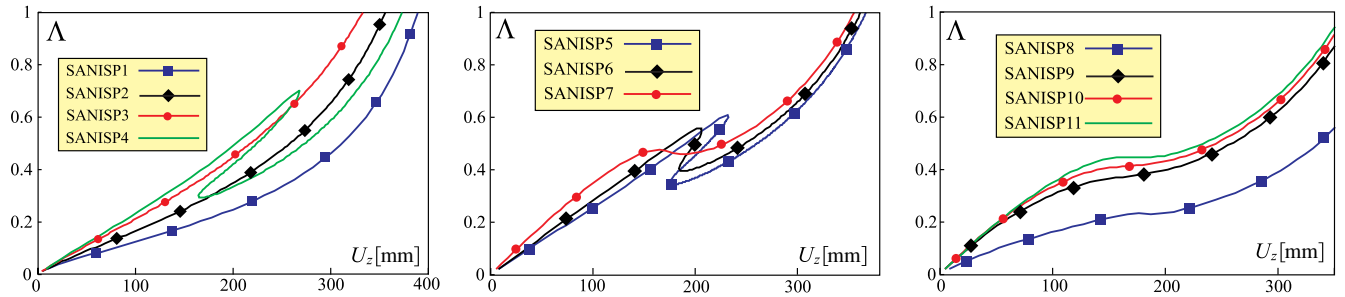

Fig. 26 Responses for different swept configurations featuring different single-layer upper wings. See Table 8 for details.

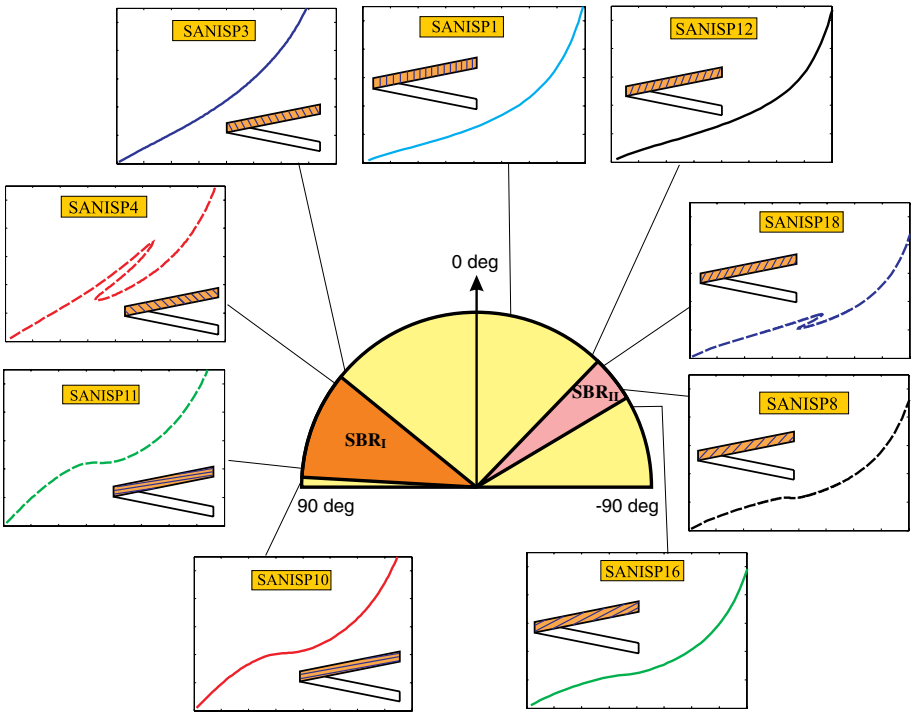

Fig. 27 Snap-buckling region and typical responses (vertical displacement of point P_1 versus load factor).

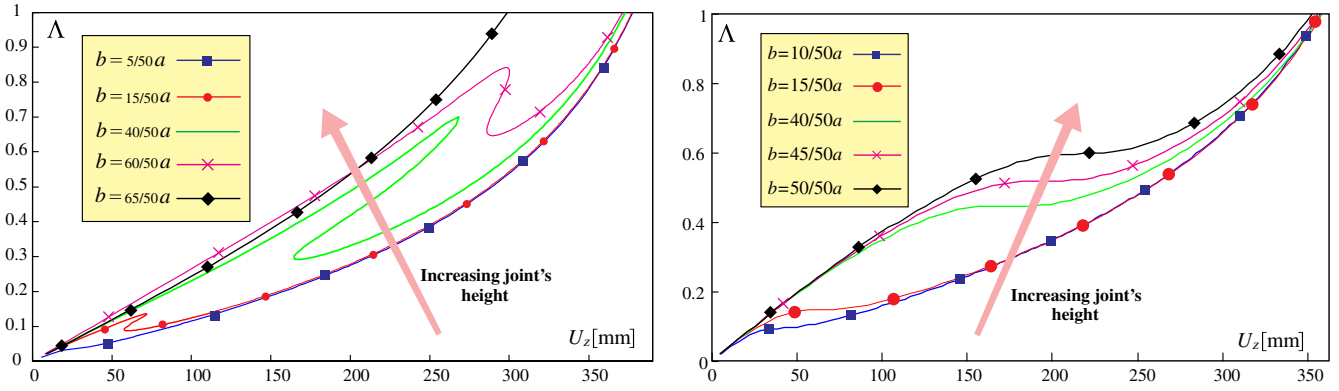

a) SANISP4 based **b) SANISP11 based**

Fig. 28 Joint's effects for the SANISP4- and SANISP11-based configurations.

VII. Conclusions

Postbuckling investigations of composite PrandtlPlane joined wings, with particular focus on the fundamental physical aspects leading to the instability and nonlinear structural response, have been presented for the first time.

Previous analyses of this innovative configuration focused on linear structural and aeroelastic models. A first attempt toward an accurate simulation and fundamental understanding of the critical and postcritical conditions has been presented in [27], where the case of isotropic materials was discussed. The effects of the geometrical parameters (joint's dimensions and sweep angles) showed a very complex nonlinear response, which could not be predicted with the standard linear analysis but needs to be properly taken into account, even at the very early stages of the design. This is particularly important, since the true critical load can often be overpredicted when a classical linear eigenvalue approach (linear buckling analysis) is adopted. Reference [27] showed that increasing the joint's height is beneficial. Moreover, it can be identified as an interval of the joint's heights in which the snap-buckling instability occurs. This was defined as the snap-buckling region. The SBR could have a significant relevance in the conceptual design of PrandtlPlane configurations, since a snap buckling type of instability must be avoided.

Reference [27] also showed that the torsional–bending coupling consequence of the geometric layout (swept wings) can dramatically worsen the stability properties. Finally, it was also presented that the load repartition between the upper and lower wings has a significant effect on the nonlinear response. In particular, for the common PrandtlPlane layout featuring a sweptback lower wing and a sweptforward upper wing, a higher percentage of the load on the upper wing was showed as reducing the risks of buckling.

However, several conceptual and theoretical aspects needed to be addressed. This was accomplished in the present work. In particular, the effect of anisotropy was extensively investigated by the adoption of composite materials. The following analyses have been carried out.

Unswept case with different isotropic materials for the upper and lower wings

An unswept joined-wing layout was investigated. Different isotropic materials were selected for the upper and lower wings. The lower-to-upper-wing stiffness ratio was shown to be the driving

parameter as far as snap-buckling instability was concerned. In particular, a counterintuitive result was found: the main mechanism that led to the instability (under nonaerodynamic conservative loads) was not due to the compression. In fact, increasing the stiffness of the upper wing via incrementing of the elastic modulus enhances the extensional stiffness (in theory, beneficial because the upper wing is compressed), but it increases the possibility of having buckling. From the Eulerian compressed column analogy, this is a highly unexpected result. The overconstrained nature of the joined wing (compared to the classical cantilevered wings) and the nonplanar geometry are responsible of this complex behavior.

Unswept case and adoption of orthotropic materials

Additional insight on the nature of the snap buckling was gained by the adoption of a single-lamina orthotropic plate for the upper wing. This choice was useful to detect which stiffness ratio was actually important for the snap-buckling occurrence. It was found that the ratio between the extensional stiffnesses and the ratio between the bending stiffnesses were the primary parameters affecting the joined wing's instability properties. As for the isotropic case, it was found that the lower wing's stiffness should be larger than the upper wing's one and the counterintuitive nature of the type of instability was confirmed. However, the single-lamina orthotropic upper wing had the drawback of presenting the lower-to-upper-wing extensional stiffness ratio equal to the lower-to-upper-wing bending stiffness ratio: it was not possible to truly separate the relative importance between the extensional and bending effects on the instability.

The problem was addressed by adopting a multilayered orthotropic laminate for the upper wing. This was very useful since, for this case, the lower-to-upper-wing extensional stiffness ratio is, in general, different than the lower-to-upper-wing bending stiffness ratio. Several investigations then showed the true driving mechanism to the instability: the snap-buckling occurrence is mainly sensitive to the lower-to-upper-wing bending stiffness ratio. In particular, it was shown that increasing the lower wing's bending stiffness was beneficial, whereas incrementing the upper wing's bending stiffness had a negative effect on the stability of the joined wing.

Type of joint's connection and its effects on snap-buckling of unswept joined wings

The bending moment transferring through the joint is one of the leading mechanisms involved in the instability. This was demonstrated by modifying the joint-to-wing connection. In particular, a quasi-hinge type of connection was implemented by inserting a hinge at the joint-to-upper-wing or joint-to-lower-wing junction and a torsional spring opposing the relative rotation between the joint and the upper/lower wing. A small value of the spring stiffness was selected, and the bending moment transferred to the upper wing was reduced compared to the fixed type of joint previously investigated. On a pure stability perspective, this provided a great benefit because the snap buckling was eventually eliminated, thus confirming the relevant importance of the bending moment transferring in the snap occurrence. As a drawback, however, the configurations with the quasi-hinge connection showed a less stiff response. Moreover, when the quasi hinge was positioned between the joint and upper wing, a softening tendency was observed in respect to the response of the configuration in which the quasi-hinge connection was established between the joint and the lower wing.

Unswept case and adoption of anisotropic materials (composites)

While the lower wing was assumed to be isotropic, the upper wing was simulated first with a multilayered orthotropic laminate and second with a multilayered anisotropic laminate presenting a identical lower-to-upper-wing bending stiffness ratio. The orthotropic case experienced a strong snap-type instability, whereas the anisotropic case did not have the instability at all in the range of explored load levels and presented a stiffening effect. Considering the fact that the geometry (unswept joined wings) does not introduce any bending–torsion coupling, whereas the anisotropic laminate does, it was deduced that the material-induced bending–torsion coupling is important in the nonlinear response.

The bending–torsion coupling was further investigated by selecting a single lamina with fibers generically oriented. The lower-to-upper-wing bending stiffness ratio and the primary bending–torsional deformation coupling term D_{26} were also monitored. The investigation showed that, in some cases, the bending–torsional coupling is beneficial; and in other cases, it deteriorates the stability properties of the joined wing. A further insight of this coupling and its effects on the instability could be gained from the observation of the joint's rotation with respect to the wingspan direction. This rotation is heavily affected by the torsional–bending coupling. In particular, a properly designed laminate could increase or decrease the rotation of the joint with enhanced or worsened stability properties.

Swept case with different isotropic materials for the upper and lower wings

The swept joined wing presents a torsional–bending coupling even if the same isotropic material is adopted for both the upper and lower wings. To gain further insight, the upper wing was selected to be isotropic but with a different elastic modulus compared to the lower wing. Several investigations showed that, to avoid snap buckling, a substantially larger lower-to-upper-wing bending stiffness ratio was necessary. A direct observation of the deformed shapes confirmed that, when this type of instability occurs, the rotation (with respect to the wingspan axis) of the joint is significant.

Swept case and torsional effects

The relative importance of torsional effects was further investigated, selecting the reference swept joined-wing configuration and changing the torsional stiffness. This was easily accomplished by adopting an orthotropic material and changing the shear modulus. When the torsional stiffness was increased, the response showed a tendency to have an abrupt snap buckling, typical of the unswept case. This should confirm that, limiting the torsional effects introduced by the geometry, the configuration tends to behave as in the unswept case.

Swept case and anisotropy effects

A physical insight on the response of PrandtlPlane joined wings was gained by the introduction of coupling effects associated with the anisotropy of the material. While the lower wing was maintained as isotropic, the upper wing was simulated with a single-ply generically oriented material. The analyses showed a very complex bending–torsion interaction: even for a relatively simple single-ply upper wing, there could be identified two distinct and unsymmetrically located regions in which the snap-buckling occurs. In other words, the snap-buckling region (i.e., range of fiber orientation's angles for which the system undergoes a snap-buckling instability) is difficult to predict from pure intuitive considerations.

Joint's height effects in the case of anisotropic swept joined wings

For the isotropic case examined in [27], the joint's height was varied, and it was found that an increase of the height was beneficial. A similar investigation has been carried out in this work with the adoption of composite materials. It was found out that the joint's height is beneficial even when the composite materials are used.

The investigations presented in this work shed some light on the very complex nonlinear response of joined wings. Results showed that the snap-buckling load is quite sensitive to the bending moment transferred by the joint to the upper wing. Thus, both the type of the joint's connection and the bending stiffness of the wings play a significant role.

When the bending–torsion coupling is introduced because of either the geometry (sweep angles) the material (composites), or both, predicting a priori if the aforementioned effects are beneficial or not is an extremely challenging task. The simulations conducted in this work seem to suggest that the rotation of the joint about the wingspan axis is an important factor for gaining further insight on instability and its properties.

Future works focusing on nonlinear effects of joined wings will discuss the theoretical challenges and physical implications when mechanical nonconservative loadings of a follower type and aerodynamic forces are taken into account. Specifically, in [36], a vortex lattice method has been used for this purpose. A further area needing some study is the characterization of stability properties under a dynamical systems perspective [34].

Acknowledgments

The authors acknowledge support by San Diego State University (College of Engineering). An earlier version of this paper (AIAA 2012-1462) was presented at the 53rd AIAA SDM conference, 23-26 April 2012, Honolulu, Hawaii, and was the recipient of the "Collier research Hypersizer AIAA Structures Best Paper" award.

References

[1] Letcher, J., "V-Wings and Diamond-Ring Wings of Minimum Induced Drag," *Journal of Aircraft*, Vol. 9, No. 8, 1972, pp. 605–607. doi:10.2514/3.59045

[2] Wolkovitch, J., "The Joined Wing Aircraft: an Overview," *Journal of Aircraft*, Vol. 23, No. 3, 1986, pp. 161–178.

[3] Lange, R. H., Cahill, J. F., Bradley, E. S., Eudaily, R. R., Jenness, C. M., and Macwilkinson, D. G., "Feasibility Study of the Transonic Biplane Concept for Transport Aircraft Applications," NASA CR-132462, 1974.

[4] Miranda, L. R., "Boxplane Wing and Aircraft," U.S. Patent 3,834,654, Sept. 1974.

[5] Frediani, A., "Large Dimension Aircraft," U.S. Patent 5,899,409, 1999.

[6] Frediani, A., "New Large Aircraft," European Patent EP-0716978B1, 20 March 2002.

[7] Livne, E., "Future of Airplane Aeroelasticity," *Journal of Aircraft*, Vol. 40, No. 6, 2003, pp. 1066–1092. doi:10.2514/2.7218

[8] Livne, E., and Weisshaar, T. A., "Aeroelasticity of Nonconventional Airplane Configurations: Past and Future," *Journal of Aircraft*, Vol. 40, No. 6, 2003, pp. 1047–1065. doi:10.2514/1.2273

[9] Prandtl, L., "Induced Drag of Multiplanes," NACA TN-182, March 1924.

[10] Scott, M., Enke, A., and Flanagan, J., "SensorCraft Free-Flying Aeroservoelastic Model Design and Fabrication," *52nd AIAA/ASME/ASCE/AHS/ASC Structures, Structural Dynamics and Materials Conference*, AIAA Paper 2011-1957, April 2011.

[11] Buttazzo, G., and Frediani, A. (eds.), *Variational Analysis and Aerospace Engineering: Mathematical Challenges for Aerospace Design Contributions from a Workshop Held at the School of Mathematics in Erice, Italy*, Springer, New York, 2012.

[12] Gern, F. H., Ko, A., Sulaeman, E., Gundlach, J., Kapania, R. H., and Haftka, R. T., "Multidisciplinary Design Optimization of a Transonic Commercial Transport with Strut-Braced Wing," *Journal of Aircraft*, Vol. 38, No. 6, 2001, pp. 1006–1014. doi:10.2514/2.2887

[13] Gur, O., Bhatia, M., Schetz, J. A., Mason, W. H., Kapania, R. K., and Mavris, D. N., "Design Optimization of a Truss-Braced-Wing Transonic Transport Aircraft," *Journal of Aircraft*, Vol. 47, No. 6, 2010, pp. 1907–1917. doi:10.2514/1.47546

[14] Reichenbach, E., Castelluccio, M., and Sexton, B., "Joined Wing Sensorcraft Aeroservoelastic Wind Tunnel Test Program," *52nd AIAA/ASME/ASCE/AHS/ASC Structures, Structural Dynamics and Materials Conference*, AIAA Paper 2011-1956, April 2011.

[15] Boston, J., Swenson, E., and Kunz, D., "Experiments with Geometric Non-Linear Coupling for Analytical Validation," *51nd AIAA/ASME/ASCE/AHS/ASC Structures, Structural Dynamics and Materials Conference*, AIAA Paper 2010-3018, April 2010.

[16] Paletta, N., Belardo, M., and Pecora, M., "Load Alleviation on a Joined-Wing Unmanned Aicraft," *Journal of Aircraft*, Vol. 47, No. 6, 2010, pp. 2005–2016. doi:10.2514/1.C000265

[17] Sotoudeh, Z., and Hodges, D. H., "Incremental Method for Structural Analysis of Joined-Wing Aircraft," *Journal of Aircraft*, Vol. 48, No 5, 2011, pp. 1588–1601. doi:10.2514/1.C031302

[18] Kim, Y. I., Park, G. J., Kolonay, R. M., Blair, M., and Canfield, R. A., "Nonlinear Response Structural Optimization of a Joined Wing Using Equivalent Loads," *AIAA Journal*, Vol. 46, No. 11, 2008, pp. 2703–2713. doi:10.2514/1.33428

[19] Chambers, J. R., Innovation in Flight: Research of the NASA Langley Research Center on Revolutionary Advanced Concepts for Aeronautics, No. 39 in Monograph in Aerospace History, NASA SP 2005-4539, Nov. 2005, pp. 227–246.

[20] Weisshaar, T. A., and Lee, D. H., "Aeroelastic Tailoring of Joined-Wing Configurations," *43rd AIAA/ASME/ASCE/AHS/ASC Structures, Structural Dynamics and Materials Conference*, AIAA Paper 2002-1207, April 2002.

[21] Demasi, L., and Livne, E., "Contributions to Joined-Wing Aeroelasticity," *International Forum on Aeroelasticity and Structural Dynamics Conference*, Seattle, WA, June 2009.

[22] Demasi, L., and Livne, E., "Exploratory Studies of Joined Wing Aeroelasticity," *46th AIAA/ASME/ASCE/AHS/ASC Structures, Structural Dynamics and Materials Conference*, AIAA Paper 2005-2172, April 2005.

[23] Demasi, L., and Livne, E., "The Structural Order Reduction Challenge in the Case of Geometrically Nonlinear Joined-Wing Configurations," *48th AIAA/ASME/ASCE/AHS/ASC Structures, Structural Dynamics and Materials Conference*, AIAA Paper 2007-2052, April 2007.

[24] Tiso, P., and Jansen, E., "A Finite Element Based Reduction Method for Nonlinear Dynamics of Structures," *46th AIAA/ASME/ASCE/AHS/ASC Structures, Structural Dynamics & Materials Conference*, AIAA Paper 2005-1867, April 2005.

[25] Tiso, P., and Rixen, D. J., "Reduction Methods for MEMS Nonlinear Dynamic Analysis," *Nonlinear Modeling and Applications*, Vol. 2, Proulx, T., Conference Proceedings of the Society for Experimental Mechanics Series, Springer, New York, 2011, pp. 53–65.

[26] Demasi, L., and Palacios, A., "A Reduced Order Nonlinear Aeroelastic Analysis of Joined Wings Based on the Proper Orthogonal Decomposition," *51st AIAA/ASME/ASCE/AHS/ASC Structures, Structural Dynamics and Materials Conference*, AIAA Paper 2010-2722, April 2010.

[27] Demasi, L., Cavallaro, R., and Razon, A., "Post-Critical Analysis of Prandtl Plane Joined-Wing Configurations," *AIAA Journal*, Vol. 51, No. 1, 2013, pp. 161–177. doi:10.2514/1.J051700

[28] Giles, L. G., "Equivalent Plate Modeling for Conceptual Design of Aircraft Wing Structures," NASA TM-111263, Sept. 1995.

[29] Stearman, R., Lin, H.-H., and Jhou, J., "Influence of Joint Fixity on the Aeroelastic Characteristics of a Joined Wing Structure," *31st AIAA/ASME/ASCE/AHS/ASC Structures, Structural Dynamics and Materials Conference*, AIAA Paper 1990-0980, April 1990.

[30] Levy, R., and Gal, E., "Triangular Shell Element for Large Rotations Analysis," *AIAA Journal*, Vol. 41, No. 12, 2003, pp. 2505–2508.

[31] Crisfield, M., *Non Linear Finite Element Analysis of Solid and Structures*, Vol. 1, Wiley, New York, 1991.

[32] Cavallaro, R., Demasi, L., and Passariello, A., "Nonlinear Analysis of PrandtlPlane Joined Wings, Part II: Effects of Anisotropy," *53rd AIAA/ASME/ASCE/AHS/ASC Structures, Structural Dynamics, and Materials Conference*, AIAA Paper 2012-1462, April 2012.

[33] Bisplinghoff, R., and Ashley, H., *Principles of Aeroelasticity*, Dover Phoenix Editions, Dover, New York, 2002.

[34] Cavallaro, R., Demasi, L., and Bertuccelli, F., "Risks of Linear Design of Joined Wings: a Nonlinear Dynamic Perspective in the Presence of Follower Forces," *54th AIAA/ASME/ASCE/AHS/ASC Structures, Structural Dynamics, and Materials Conference*, AIAA Paper 2013-1558, April 2013.

[35] Blair, M., Canfield, R. A., and Roberts, R. W. Jr., "Joined-Wing Aeroelastic Design with Geometric Nonlinearity," *Journal of Aircraft*, Vol. 42, No. 4, 2005, pp. 832–848.

[36] Demasi, L., Cavallaro, R., and Bertuccelli, F., "Post-Critical Analysis of Joined Wings: the Concept of Snap-Divergence as a Characterization of the Instability," *54th AIAA/ASME/ASCE/AHS/ASC Structures, Structural Dynamics, and Materials Conference*, AIAA Paper 2013-1559, April 2013.

W. Silva
Associate Editor